LEVEL

TECHNICAL
MEMORANDUM
NCSC TM220-78

AUGUST 1978

UNDERWATER JETTING
AND A JET/DIRECT TOOL
FOR INVESTIGATION

C. SMITH

NAVAL COASTAL SYSTEMS CENTER
PANAMA CITY, FLORIDA 32407

NAVAL COASTAL SYSTEMS CENTER

PANAMA CITY, FLORIDA 32407

CAPT JAMES V. KELLEY, USN
Commanding Officer

GERALD G. GOULD
Technical Director

ADMINISTRATIVE INFORMATION

This study (Task No. XR-7-003-2 was accomplished under Civil Engineering Laboratory's (CEL's) NAVFACENGCOM Block Program. The task was intended to establish basic design information in the development of a diver operated jetting device.

UNCLASSIFIED

SECURITY CLASSIFICATION OF THIS PAGE *(When Data Entered)*

REPORT DOCUMENTATION PAGE	READ INSTRUCTIONS BEFORE COMPLETING FORM
1. REPORT NUMBER: NCSC-TM-229-78	2. GOVT ACCESSION NO. / 3. RECIPIENT'S CATALOG NUMBER
4. TITLE *(and Subtitle)*: UNDERWATER JETTING AND A JET/DREDGE TOOL FOR DIVER USE	5. TYPE OF REPORT & PERIOD COVERED: Technical Memorandum
	6. PERFORMING ORG. REPORT NUMBER
7. AUTHOR(s): Carl Smith, John Mittleman	8. CONTRACT OR GRANT NUMBER(s)
9. PERFORMING ORGANIZATION NAME AND ADDRESS: Naval Coastal Systems Center, Panama City, Florida 32407	10. PROGRAM ELEMENT, PROJECT, TASK AREA & WORK UNIT NUMBERS: WR-7-0042
11. CONTROLLING OFFICE NAME AND ADDRESS	12. REPORT DATE: August 1978
	13. NUMBER OF PAGES: 48
14. MONITORING AGENCY NAME & ADDRESS *(if different from Controlling Office)*	15. SECURITY CLASS. *(of this report)*: UNCLASSIFIED
	15a. DECLASSIFICATION/DOWNGRADING SCHEDULE: N/A

16. DISTRIBUTION STATEMENT *(of this Report)*

Approved for Public Release; Distribution Unlimited.

17. DISTRIBUTION STATEMENT *(of the abstract entered in Block 20, if different from Report)*

18. SUPPLEMENTARY NOTES

19. KEY WORDS *(Continue on reverse side if necessary and identify by block number)*

Diver equipment
Seafloor construction equipment
Dredging
Underwater

Identifiers:
Underwater jetting
Diver tools
Working diver
Jetting

20. ABSTRACT *(Continue on reverse side if necessary and identify by block number)*

Underwater jetting and dredging components were tested to determine their hydrodynamic characteristics. The components were combined to form a three-way combination system of a single jet, a single dredge, and a combination jet-dredge system. The operational characteristics of these three configurations were then determined by testing their ability to excavate the sandy sediments in the waters off Panama City, Florida. The single jet system rapidly fluidized the sand, but did not transport it effectively; the single dredge

DD FORM 1 JAN 73 1473 EDITION OF 1 NOV 65 IS OBSOLETE
S/N 0102-LF-014-6601

UNCLASSIFIED
SECURITY CLASSIFICATION OF THIS PAGE *(When Data Entered)*

410 650

20.

cont'

system transported the sand effectively but required constant attention to prevent clogging the suction. The combination jet-dredge system gave the best overall excavation rate and required less work from the diver than either single component system. The combination is also a force-balanced system requiring little diver effort to handle the device.

Correlation between soil properties and stagnation pressure were successful in establishing preliminary guidelines for choosing a nozzle, if the characteristics of the bottom material are known.

ASSISTANT

SUMMARY

The Civil Engineering Laboratory (CEL), Port Hueneme, California tasked Naval Coastal Systems Center with testing and evaluating underwater jetting and dredging components with a final goal of fabricating a prototype diver operated combination jet/dredge. Tests were carried out on a pump and various sizes of nozzles in order to establish design procedures for selection of the most efficient nozzle for use in a given bottom material.

Upon completion of the nozzle tests a prototype jet/dredge combination tool was assembled using a Stanley SM-22 sump pump which supplied power to the nozzle and a 3-inch "Gold Dredge." This size dredge was chosen because of it's power input requirements and immediate availability. Tests were then completed on the combination jet/dredge and it's performance in different bottom materials recorded.

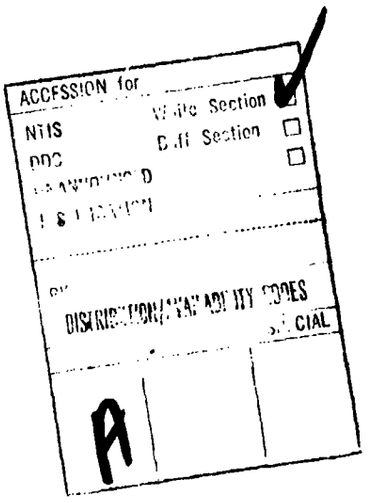

(Reverse Page ii Blank)

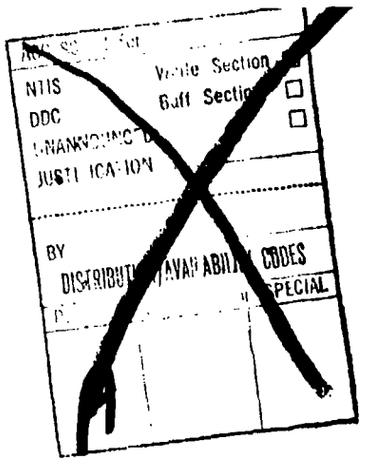

TABLE OF CONTENTS

TABLE OF CONTENTS (CONT'D)

LIST OF ILLUSTRATIONS

LIST OF TABLES

INTRODUCTION

The construction, maintenance, and repair of fixed ocean facilities is a mission of the Naval Facilities Engineering Command supported by the Civil Engineering Laboratory (CEL) and the underwater construction teams. Many construction tasks require removal of sediments. Jetting and dredging are the most commonly used techniques. Pipeline, cable emplacement, and placement of mooring systems for ships and buoys, are tasks where some type of water jet may be used to accomplish the job. Small salvage operations may require the use of a jet and/or dredge. The inspection and repair of pipeline or cable systems may also require a jet or dredge.

Present methods for jetting require the diver to contend with large heavy hoses, unbalanced forces, and in some cases poor visibility. Where dredging is used, the task of handling awkward sump pumps often results in excessive diver fatigue. Also, since sump pumps have a limitation on the size of solids they can safely pump in a slurry, the diver must remove shells, small stones, and other debris to prevent clogging. CEL tasked NCSC to establish a basis for improvement in jetting and dredging hardware.

The preliminary phase of the project involved gathering basic hydrodynamic data of various sized nozzles. This was done because of the lack of design information available in the area. An example of a nozzle which does not take full advantage of the power available from the pump is the ½-inch balanced nozzle which is included in the tool kit assembled at NCSC. This nozzle size may serve its purpose if used in clay type sediments where a cutting action is required, but if used in soft sand that can easily be fluidized, this nozzle would not be the most efficient. In order to gather data on these components a lightweight test frame was constructed on which a pump, flowmeter, and nozzles were mounted (Figure 1).

EXPERIMENTAL OBJECTIVES AND APPROACHES

A series of experiments were performed to gather basic hydrodynamic data describing the performance of various jetting system components. These experiments are divided into the following groups:

(Text Continued on Page 3)

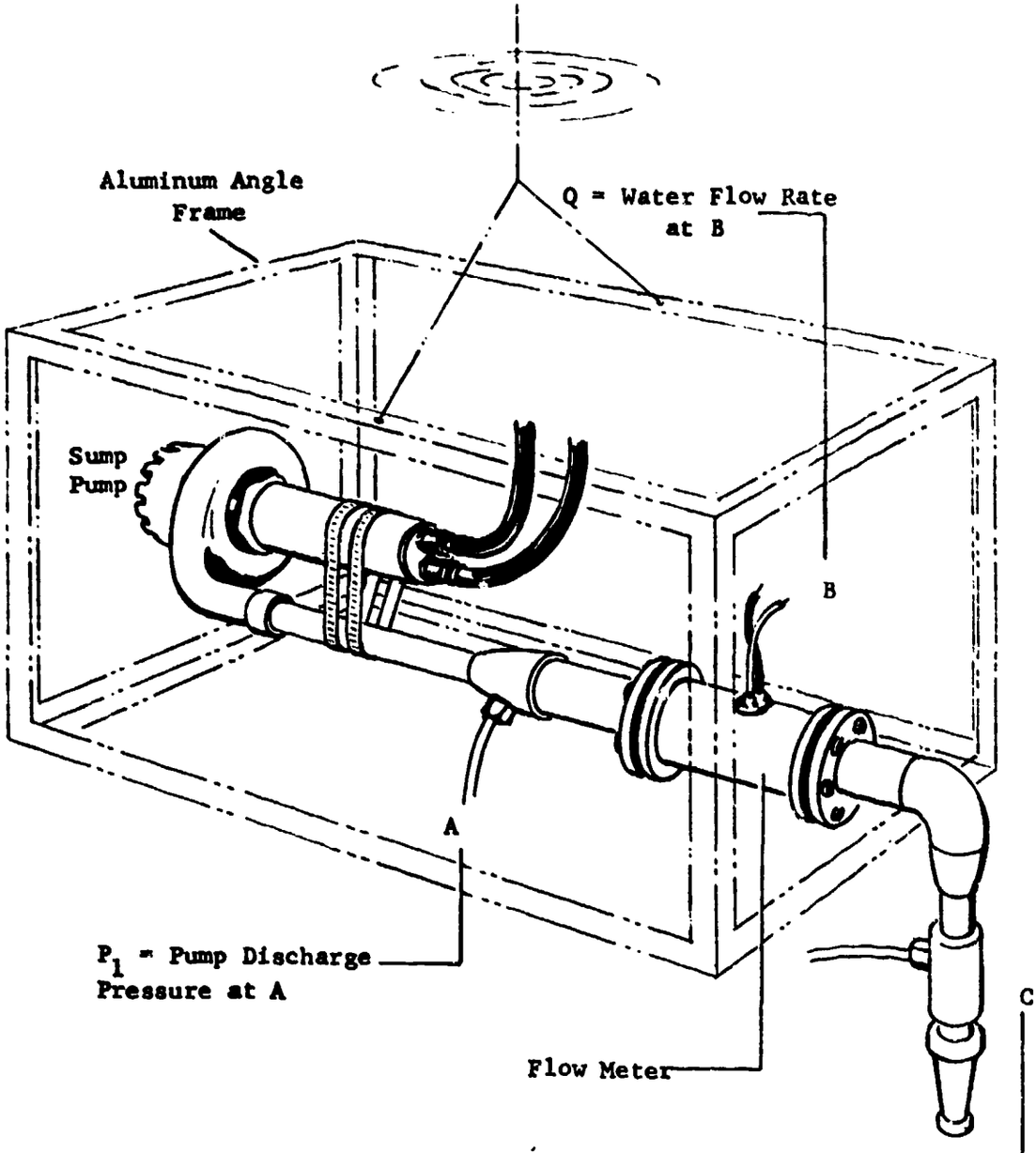

FIGURE 1. FLOW AND PRESSURE TEST SETUP

1. HYDRODYNAMIC DESCRIPTIONS

   - hydraulic sump pump
   - test rig piping
   - jetting nozzles

2. OPERATIONAL DESCRIPTION

   - excavation rates
   - reaction forces
   - jet/dredge experiences

The majority of tests were run with the components mounted in the test frame constructed of lightweight aluminum angle stock (Figure 1).

HYDRODYNAMIC DESCRIPTIONS

Hydraulic Sump Pump

The objective of the first set of tests was to characterize the hydraulic sump pump (Stanley Model SM22) with a series of flow versus pressure curves for various hydraulic supply conditions. For these experiments the nozzle and pressure tap (location C) shown in Figure 1 were replaced by a gate valve so that a range of back pressures could be imposed on the pump. Then, for hydraulic flow rates between 5 and 10 gallons per minute (18.9-37.9 lpm) the water flow rate (Q), pump discharge pressure (P_1), and ambient pressure (P_a) were measured. Pump discharge pressure was sensed at location A, water flow rate at location B and downstream pressure (P_2) at location C. Further, the pressure gauge at location A was left in the system throughout all nozzle tests so that additional pump data could be collected using the nozzles rather than the gate valve, as a flow restriction.

Test Rig Piping

The second set of tests characterized the piping between the pump and the nozzle under test. Actually, these data were collected during the pump and nozzle tests by noting the pressure drop between pressure gauge at location A and the end of the test rig pipe section. During pump tests the end of the pipe section was open to ambient pressure, and during the nozzle tests the end of the test rig piping was at location C (the downstream pressure gauge).

Jetting Nozzles

The third set of experiments characterized the flow and pressure relationship for nozzles. The nozzles tested were:

- 1/2" straight pipe
- 3/4" straight pipe
- 1" straight pipe
- 1¼" straight pipe

} with bell reducer (1½ x 1¼ and appropriate reducing bushings

- 1/2" orifice tapered nozzle (Halperin part # NT202)
- 3/4" orifice tapered nozzle (Halperin part # NT202)
- 1" orifice tapered nozzle (Halperin part # NT202)
- 1 1/8" orifice tapered nozzle (Halperin part # NT202)
- 1 1/4" orifice tapered nozzle (Halperin part # NT202)

The data which characterize these nozzles are the water flow rate, (Q), and the pressure drop across the nozzle (this is computed as the difference between the gauge pressure, (P_2), and ambient pressure (P_a).

TEST PLAN

EXCAVATION RATES

The first set of tests in the operational category were intended to compare the excavation rate of each nozzle under various supply conditions. The test stand was modified by the addition of flotation which permitted it to be moved in the water quite easily. For each test, the test stand was positioned over an undisturbed section of the sand bottom off NCSC's east pier, with the nozzle pointing straight down. The bottom was jetted for 1 minute. Measurements of the diameter and depth of the jetted hole were then recorded. Because the sand in this area fluidized easily and recompacted slowly, the data gathered by these experiments should be interpreted as volume fluidized rather than excavated. Subsequent excavation rate tests were performed, allowing sufficient time for the fluidized material to settle.

REACTION FORCES

The second set of tests was an evaluation of reaction forces resulting from use of various nozzles. Early in the project it was thought that if the test stand and piping were physically constrained then the nozzle reaction would be seen as a compressive force in the pipe just upstream of the nozzle. An annular load cell was built and installed in the pipe to measure this force. When this apparatus was tried, it indicated that the pipe was in tension rather than compression. Thinking through this problem again led to the realization that the static pressure in the pipe (essentially what is read on pressure gauge at location C) creates a tensile condition greater than the compressive force attributable to the change of momentum term. Further, since the net contribution of static pressure terms must be zero for the entire system (refer to Appendix A), the reaction force relates only to the change in momentum term

$$\frac{d(mv)}{dt} = v\frac{dm}{dt} = v(\rho vA) = \frac{\rho Q^2}{A}$$

where

$\frac{d}{dt}$ = differentiation with respect to time

m = mass

v = velocity

A = orifice area

Q = flow rate

and ρ = density .

To perform the reaction force studies (after abandoning the load cell), the test rig was suspended with the nozzle pointing straight down and forces were measured with a Chatillion Scale (Figure 2).

JET AND DREDGE TESTS

The intent of these tests was to gather information relating to the advantage (or disadvantages) of combining the pump, jet, and dredge into a single tool which would be the deliverable hardware of this project.

(Text Continued on Page 7)

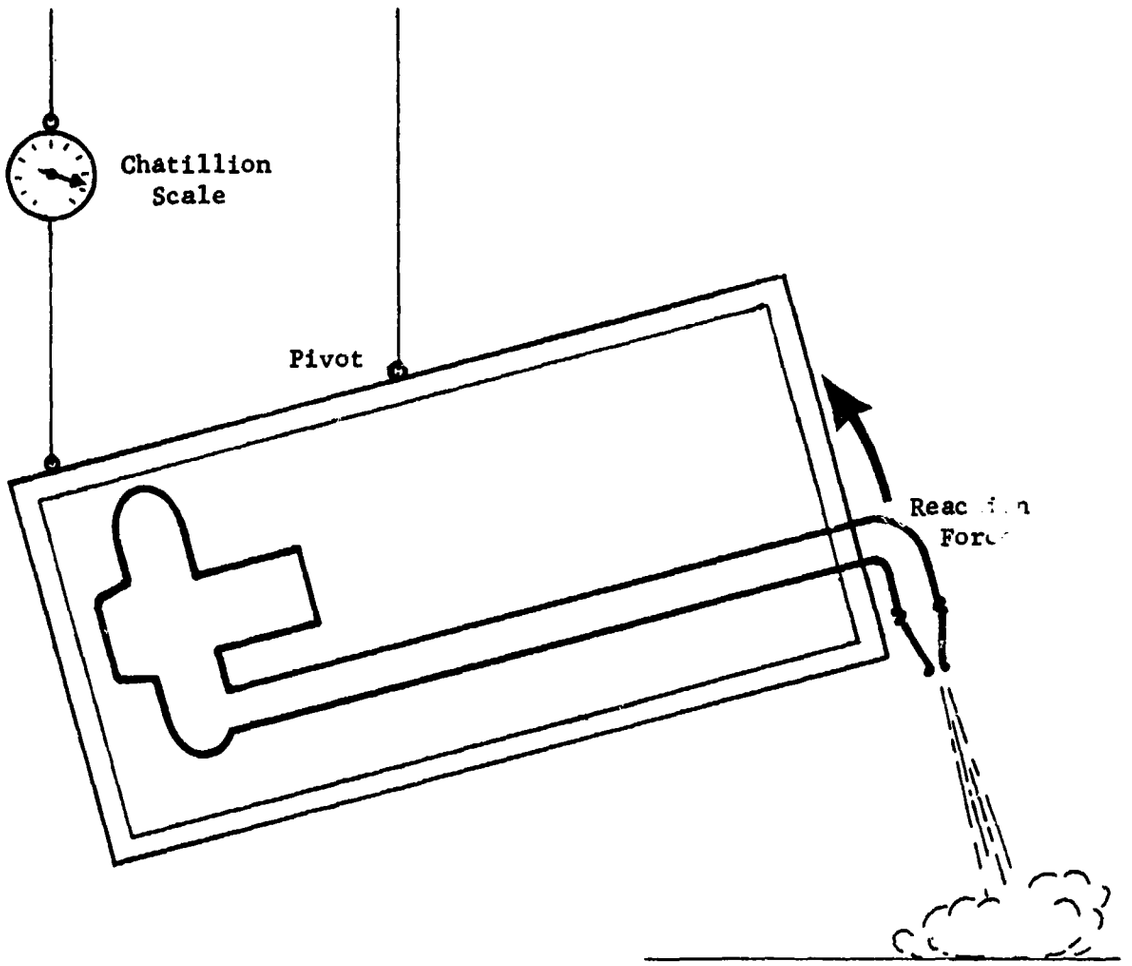

FIGURE 2. REACTION FORCE MEASUREMENT SETUP

EXPERIMENTAL RESULTS

HYDRAULIC SUMP PUMP

Data obtained from pump tests comprise a set of characteristic curves (flow versus pressure) for hydraulic fluid supply flow rates between 5 and 10 gpm (3.9 and 18.9 lpm) (Figure 3). Several cautionary notes are in order.

1. Repeatability. Setting a desired hydraulic fluid flow rate on the power source does not guarantee that the sump pump will operate along the corresponding curve shown in Figure 3. To show the magnitude of this problem Figure 4 presents all pump characteristic data points corresponding to a nominal hydraulic flow rate of 10 gpm (18.9 lpm). Efforts were made to keep the hydraulic fluid at a constant temperature by installing 100 feet of hose from the power source to the pump, and by putting a large portion of this hose in the water to cool the hydraulic fluid; but supply conditions still varied as shown in Figure 4. Examination of Figure 5 shows the range of flow and pressure in hydraulic fluid encountered during the tests and demonstrates that these parameters seemingly do not systematically depend upon hydraulic fluid temperature.

2. Similarity. The affinity laws for centrifugal pumps predict that all characteristic curves for a particular pump are related through the reduced flow and pressure variables.

$$\frac{Q}{\eta} \text{ and } \frac{P}{\eta^2}$$

where

η = impeller speed .

Under the assumption that the sump pump's motor speed is directly proportional to hydraulic fluid flow rate, the affinity laws' applicability was tested by redrawing the curves of Figure 3 on reduced axes of

$$\frac{Q_{water}}{Q_{hydraulic}} \text{ and } \frac{P_1}{Q^2_{hydraulic}} .$$

These reduced characteristic curves are presented in Figure 6. The curves do not follow the affinity laws' as well as one might hope.

(Text Continued on Page 12)

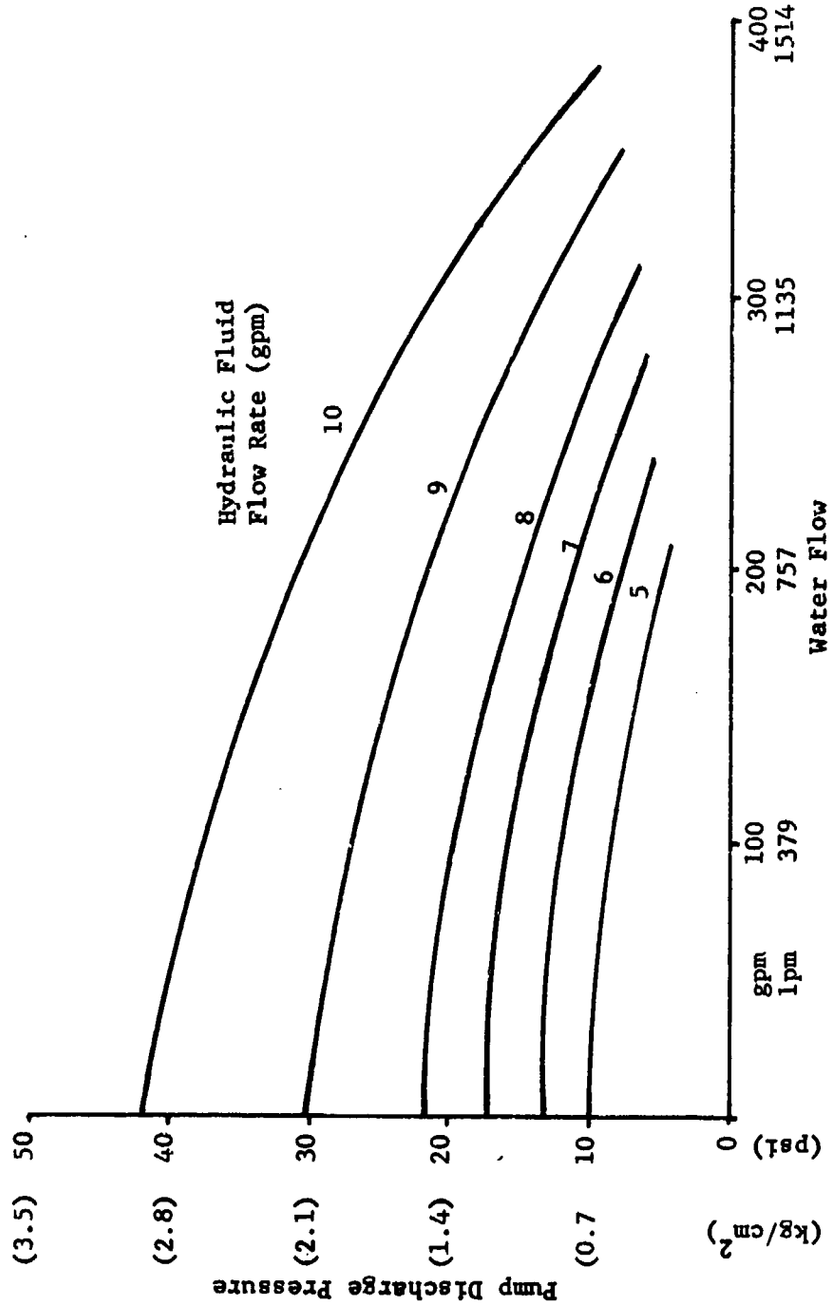

FIGURE 3. SUMP PUMP CHARACTERISTIC CURVES

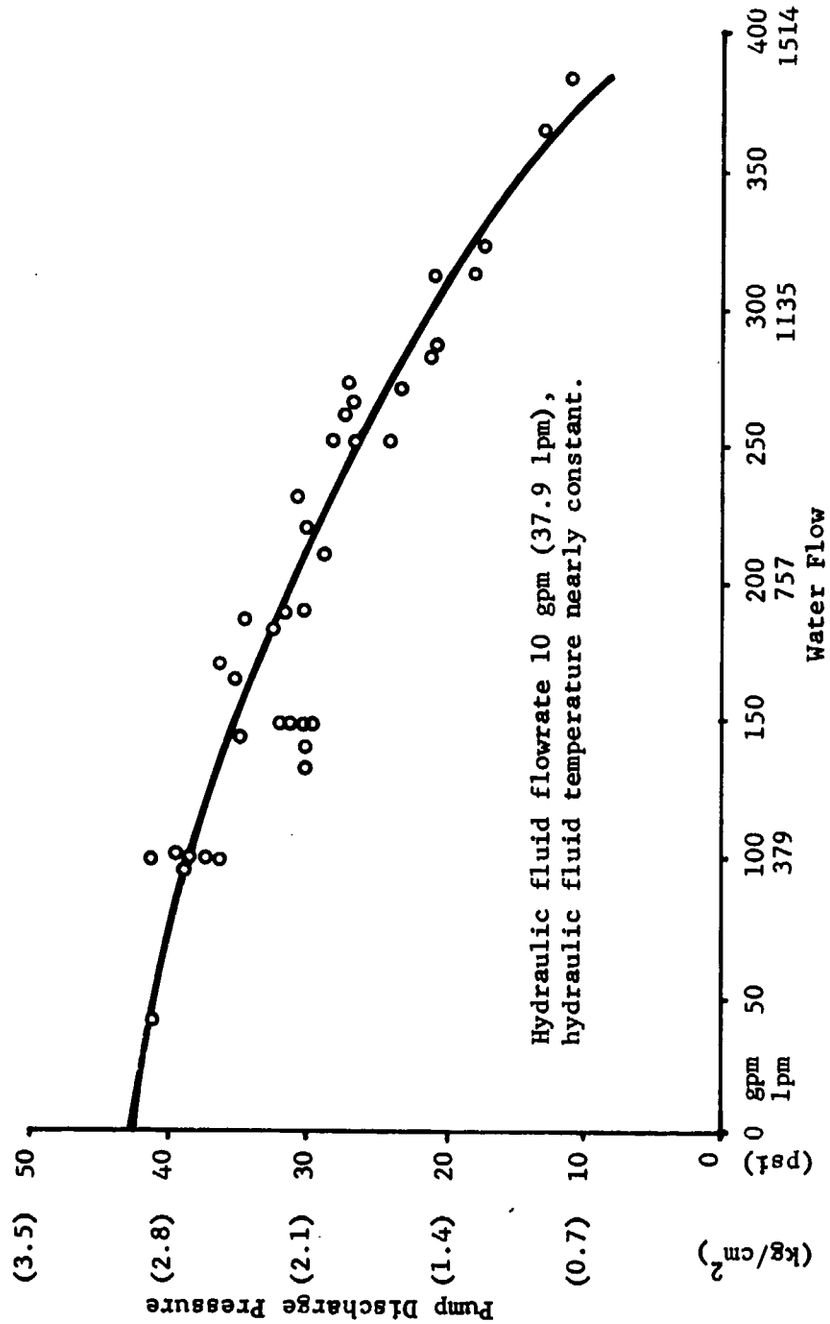

FIGURE 4. WATER FLOW VERSUS PUMP PRESSURE

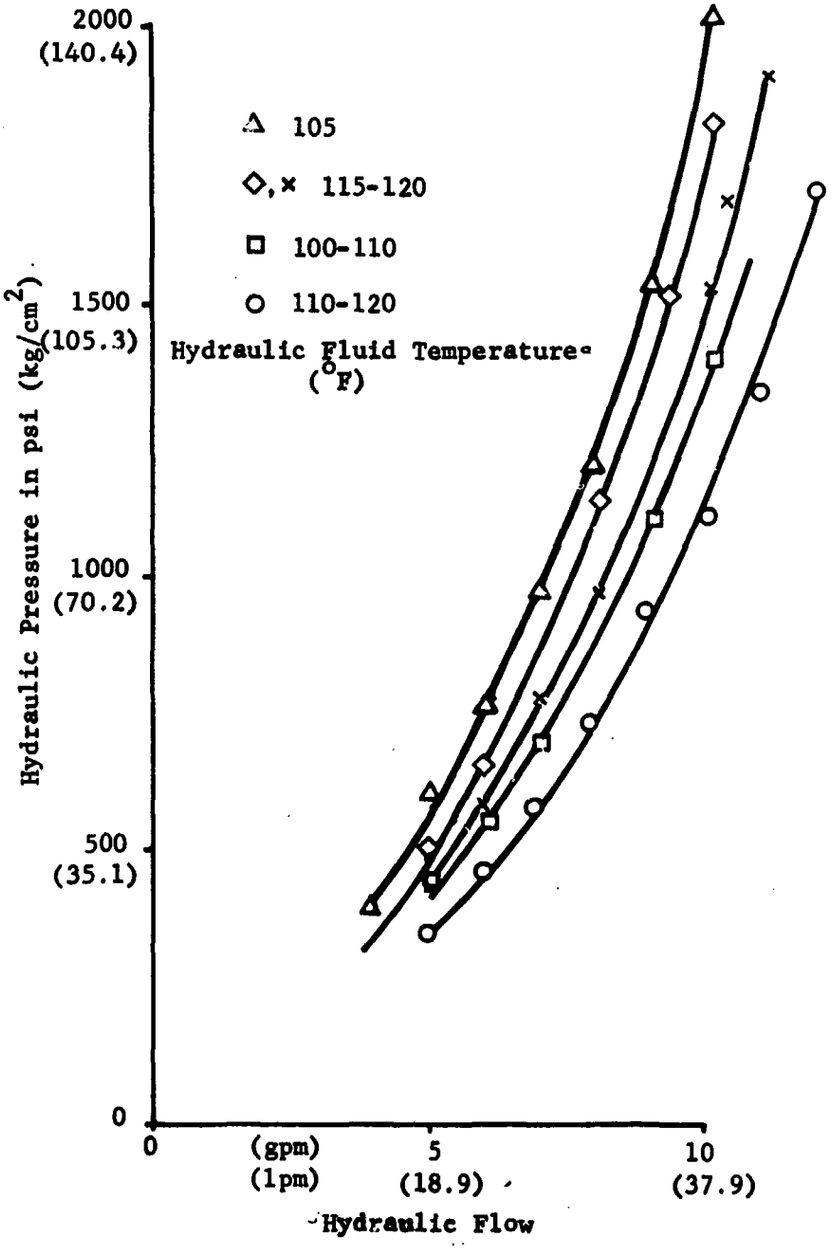

FIGURE 5. HYDRAULIC FLUID PRESSURE VARIATIONS DUE TO TEMPERATURE

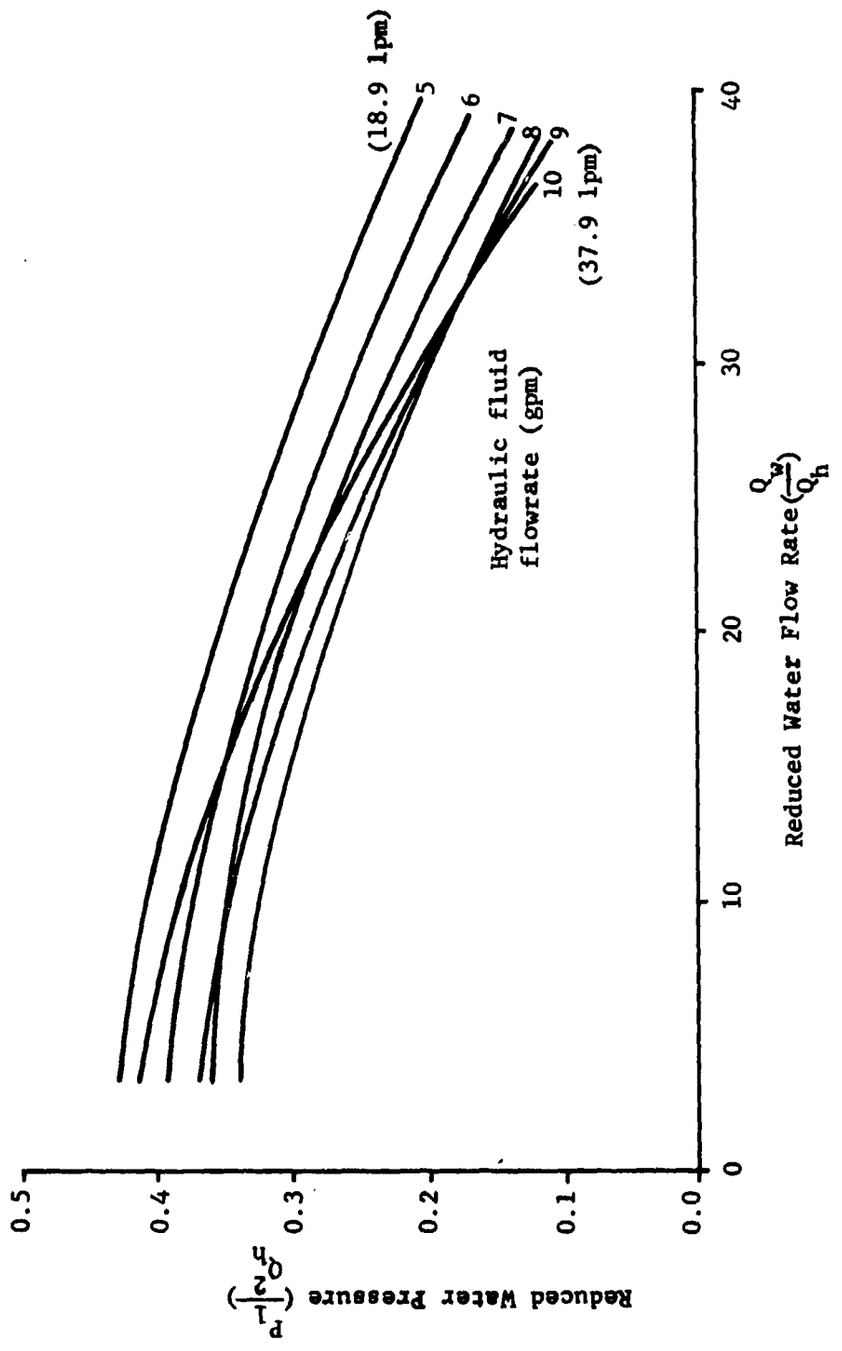

FIGURE 6. REDUCED CHARACTERISTIC CURVES

TEST RIG PIPING

During nozzle tests the pump discharge pressure at A (Figure 1) (P_1) was measured to provide additional pump data and the discharge flow pressure (P_2) at the nozzle (C in Figure 1) was measured to determine certain nozzle characteristics. The difference between these two pressures is the pressure drop in the test rig piping. A total of 69 data points were used to determine that for the test rig piping the difference in pressure was

$$\Delta P = (1.75 \times 10^{-4})Q^2 \quad \frac{\text{psi}}{(\text{gpm})^2} \quad .$$

Although this information is applicable only to the test rig, it does point out that for systems design, the piping between the pump and the nozzle must be considered, either by adding it to the nozzle characteristic or by subtracting it from the pump characteristic.

JETTING NOZZLES

The straight and tapered nozzles listed in the subsection on Jetting Nozzles were tested to establish their pressure versus flow relationship characteristics. For flow through an orifice the pressure could be expected to be proportional to the square of the flow rate; this hypothesis was tested and found to be quite reasonable. Figure 7 shows the pressure-flow curves for each nozzle tested.

EXCAVATION RATES

Discussion

The process of excavating sand may be thought of in terms of two distinct mechanisms; i.e., fluidizing and transporting, which act together. In the early excavation rate tests, the experimental setup of Figure 1 was used, and after jetting for 1 minute, the dimensions of the resulting hole in the sand were measured. At the time the measurements were taken the sand was fluidized, but not necessarily removed from the hole. Therefore, the early results only report the volume of sand fluidized. The fluidized material remained in this state approximately one-half hour after the hole was produced. Later tests both with and without the dredge operating took this into account by allowing sufficient time for recompaction of the fluidized sand.

(Text Continued on Page 14)

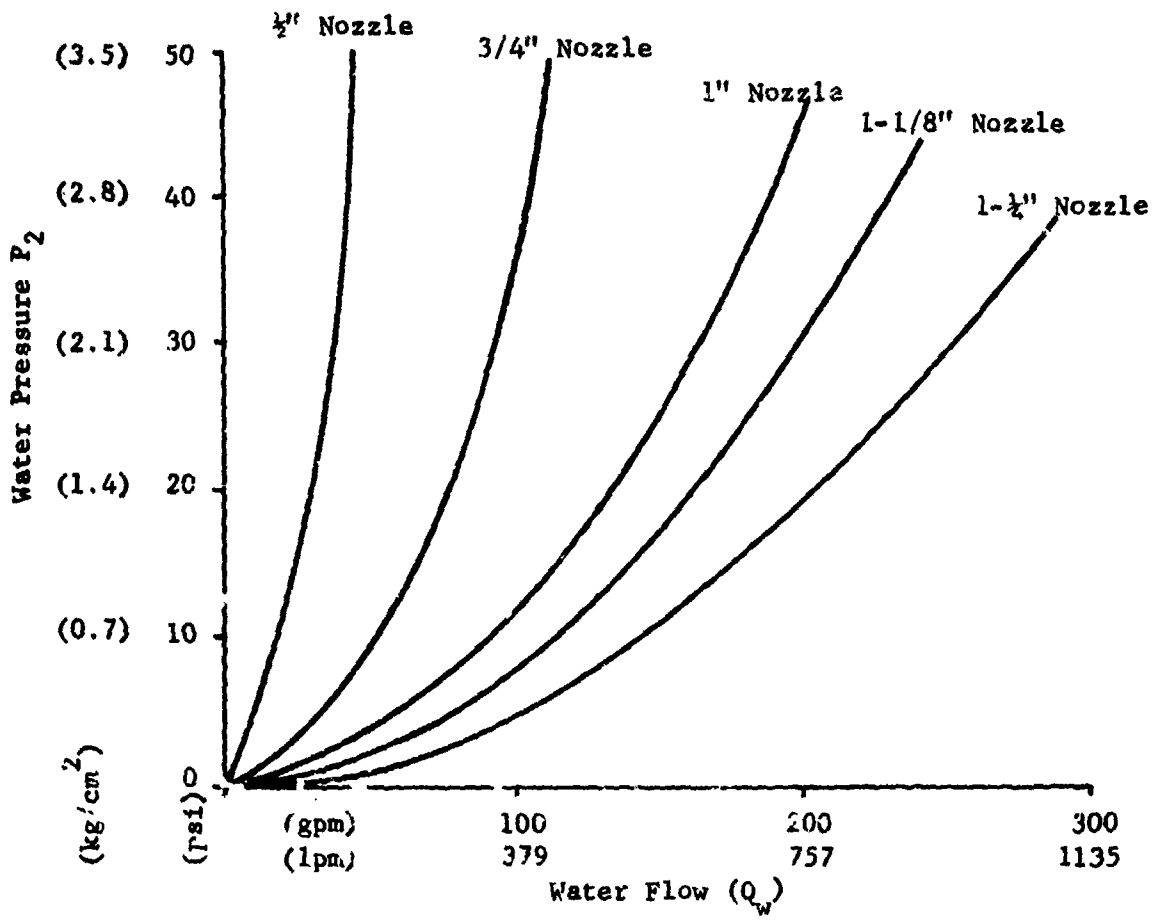

FIGURE 7. CHARACTERISTIC CURVES OF JETTING NOZZLES

Fluidization

Assuming that fluidization occurs when the jet's stagnation pressure reaches or exceeds some value related to the sediment's shear strength the early jetting results can be analyzed in terms of the theory of turbulent jets; this theory allows calculation of the stagnation pressure at various distances from the nozzle and should, therefore, allow predictions of the maximum distance from the nozzle where sand will be fluidized.

The theory predicts that the variation of flow velocity on a jet axis is related to the distance from the "pole" of the jet by an equation of the form

$$v = \frac{m}{x}$$

and stagnation pressure by an equation of the form

$$P_s = \frac{k}{x^2} .$$

In the latter equation, k may be determined experimentally, as may be the additive constant relating the pole position to the nozzle position. Theoretical values are also available.

In Appendix B the theoretical values taken from Reference 1 and the experimental values taken from Reference 2 are shown to be in reasonably good agreement and produce the following equation:

$$P_s = P_o\left[\frac{47}{\left(\frac{x}{D} + 2.1\right)^2}\right]$$

where x is measured from the nozzle's orifice.

The hypothesis that fluidization will occur if the stagnation pressure (P_s) exceeds a value related to the sediment's shear strength may now be tested by calculating the stagnation pressures found at the maximum observed depth of a jetted hole.

---

(1) Abramovich, G. N., *The Theory of Turbulent Jets*, M.I.T. Press, Cambridge, MA., 1963.

(a) Cheung, J. B., et al, *Study on Water Jet Trenching, Flow Technology*, Presentation #2, Flow Research, Inc., Kent, Washington, 3 December 1976.

Table 1 presents data collected during excavation rate studies, with estimates of the initial nozzle pressure obtained by overlaying Figure 3 (sump pump characteristics) on Figure 7 (nozzle flow and pressure). The last column of Table 1 shows values of stagnation pressure calculated at the bottom of the jetted hole. A histogram of these last data is plotted in Figure 8 to show that they are normally distributed about a mean stagnation pressure of 0.49 psi (with a standard deviation of 0.15 psi). Also shown on Figure 8 is a smoothed sample distribution (a Hanning window was used in smoothing) and a normal distribution curve having the appropriate mean and standard deviation.

Since the shear strength of the sandy soil which was fluidized was approximately 0.17 psi (0.01 kg/m^2), it appears that these sediments fluidize when the stagnation pressure is on the order of three times the shear strength. It should be recognized that part of the variability in the data is attributable to experimental uncertainties (particularly the estimations for the initial nozzle pressure), and to variations in the soil properties. Although no attempt was made to sort out these factors, it seems clear that the techniques of analysis used here could be reversed to provide reasonably good estimates of the depth of fluidization that a given nozzle will achieve. This is discussed further in the section dealing with design procedures.

EXCAVATION RATES

While fluidization appears to be predictable on the basis of theory, it is not so clear that excavation is easily predictable. Once the sand particles are dislodged by a jet, the mechanics of sediment transport come into play to determine whether or not these particles will make it out of the hole or not. Data relative to the jetting-dredging tests are shown in Table 2. Table 3 lists the excavation effectiveness of jetting alone and for the jet-dredge combination. Comparing the fluidized volume with the volume after settling, each test with the jet alone shows that only 25 percent of the fluidized volume was permanently removed from the hole. Though it may be coincidence that this percentage is so constant over a wide range of nozzle sizes it could be that it is dependent on sediment properties. Not enough quantitative data were gathered to justify further conclusions on excavation rates by jetting alone.

REACTION FORCES

Examination of Table 4 and Figure 9 (nozzle reaction forces, F_x) shows that through the use of the change in momentum equation,

$$\frac{d(mv)}{dt} = \frac{\rho Q^2}{A} ,$$

(Text Continued on Page 18)

TABLE 1

EXCAVATION DATA

Nozzle Size & Type	Hydraulic Flow Rate (gpm)	Observed Depth of Hole (inches)	Inferred Source Pressure (psi)	Calculated Stagnation Pressure (psi)
1 1/4" Tapered	10	58, 60, 58	27	0.54, 0.51, 0.54
	9	56, 54, 53	21	0.45, 0.48, 0.50
	8	54, 48, 46	16	0.37, 0.46, 0.50
	7	43, 40, 39	13	0.46, 0.53, 0.55
	6	39, 39, 37	11	0.47, 0.47, 0.51
	5	36	8	0.39
1 1/8" Tapered	10	55, 54, 54	30	0.54, 0.56, 0.56
	9	45, 49, 50	23	0.61, 0.52, 0.50
	8	44, 45, 45	17.5	0.58, 0.46, 0.46
	7	39, 40, 38	15	0.48, 0.50, 0.55
	6	38, 37, 29	12	0.44, 0.46, 0.73
	5	34	9	0.40
1" Tapered	10	65, 54, 53, 54	32	0.33, 0.48, 0.50, 0.48
	9	60, 44, 42, 50	24.5	0.30, 0.54, 0.59, 0.42
	8	52, 41, 38, 49	18	0.29, 0.46, 0.53, 0.32
	7	48, 38, 35, 41	16	0.30, 0.47, 0.55, 0.40
	6	33, 34, 34, 40	12	0.46, 0.43, 0.43, 0.32
	5	35, 33	9	0.31, 0.34
3/4" Tapered	10	60, 35, 30	34	0.24, 0.67, 0.90
	9	53, 28, 28	27.5	0.24, 0.83, 0.83
	8	50, 30, 21	22	0.22, 0.58, 1.14
	7	37, 24, 24	17	0.30, 0.69, 0.69
	6	27, 20, 18	14	0.45, 0.80, 0.97
	5	26	10	0.35
1/2" Tapered	10	36, 30, 28	40	0.34, 0.49, 0.56
	9	28, 24, 23	31	0.43, 0.58, 0.63
	8	26, 26, 25	23	0.37, 0.37, 0.40
	7	22, 20, 20	19	0.42, 0.50, 0.50
	6	16, 18, 18	15	0.61, 0.49, 0.49
	5	-	12	-
1 1/4" Pipe	10	69	35	0.50
	9	56	21	0.45
	8	50	16	0.42
	7	46	13	0.40
	6	36	11	0.54
	5	36	8	0.39
1" Pipe	10	48	32	0.60
	9	46	24.5	0.50
	8	43	18	0.42
	7	39	16	0.45
	6	32	12	0.49
	5	30	9	0.41
3/4" Pipe	10	40	34	0.52
	9	40	27.5	0.42
	8	33	22	0.49
	7	33	17	0.38
	6	24	14	0.57
	5	19	10	0.62

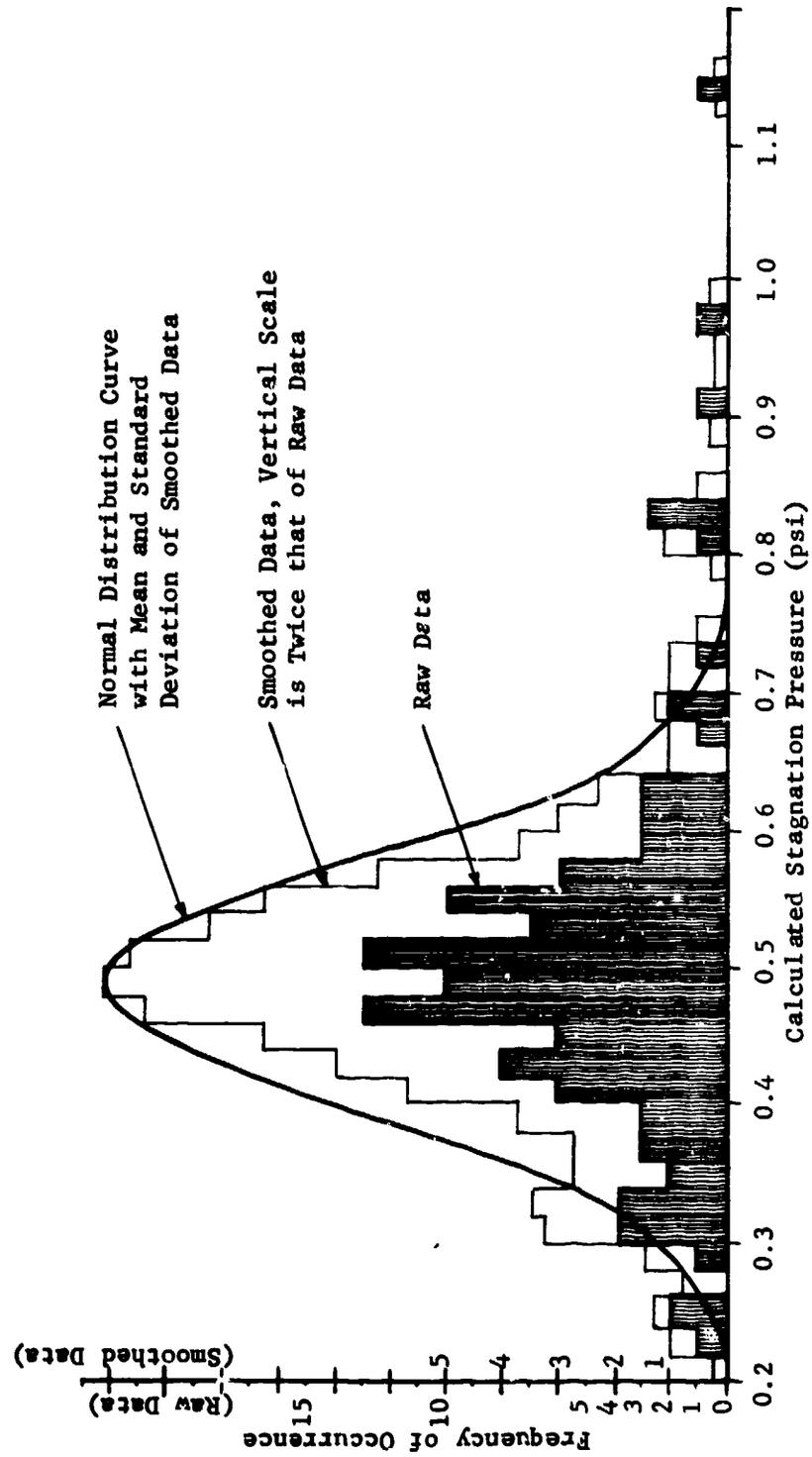

FIGURE 8. HISTOGRAM OF CALCULATED STAGNATION PRESSURE

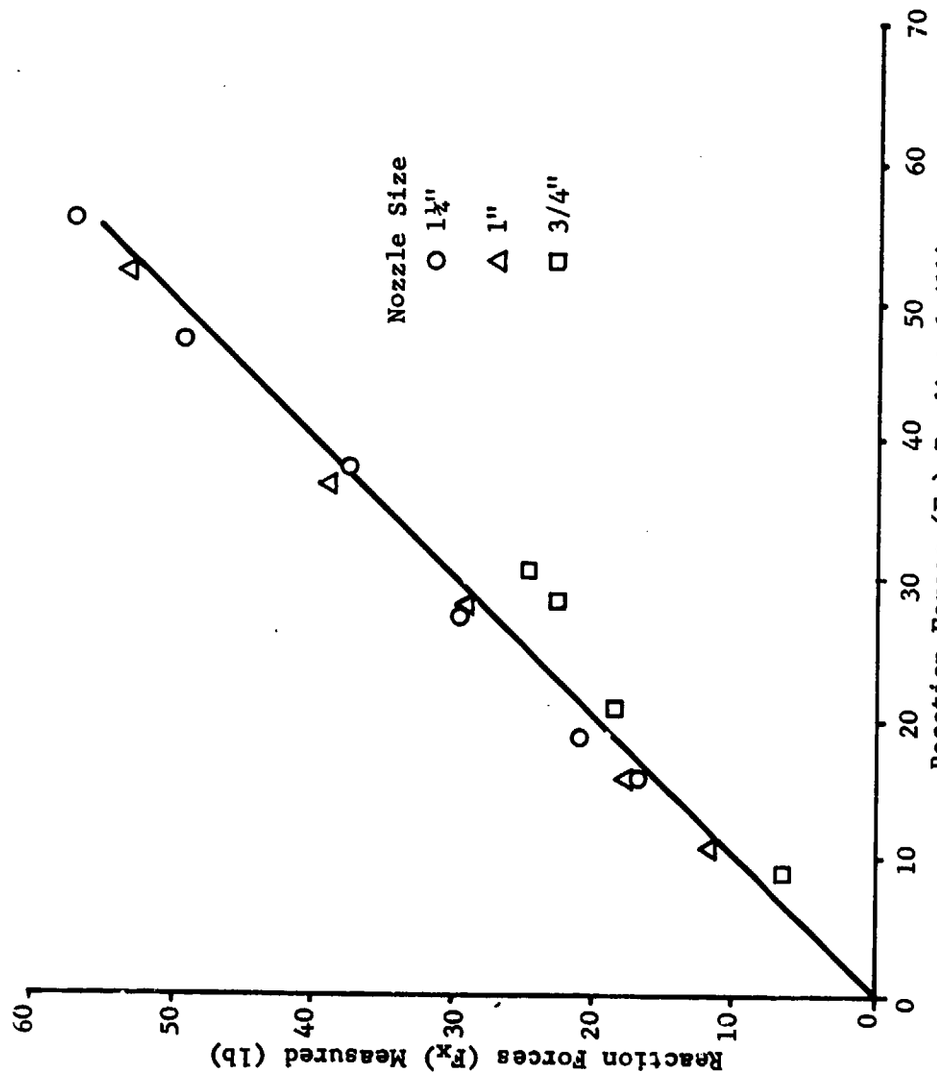

FIGURE 9. NOZZLE REACTION FORCES

TABLE 2

TEST SITE DATA

	Sand	Clay
Location	East Pier	Jetties (N.W. of Buoy #9)
Water Depth	≈ 15	≈ 35
Sea Floor Material Classification	Silty Sand	Silty Clay
Sea Floor Material Properties		
a. Density b. Shear Strength (vane shear)	1.75 g/cc 12 g/cm^2	1.878 g/cm^3 5.76 g/cm^2

predictions of the reaction forces produced by various sizes of nozzles can be obtained with reasonable accuracy. These reaction force measurements were obtained using the configuration in Figure 2.

JET-DREDGE TESTS

Quantitative Results

Figures 10 and 11 are photographs of the combination jet-dredge tool that was built.

Table 3 shows volumes of sand fluidized and completely removed by the jet-dredge combination and the jet alone. The percentage of material fluidized by the jet-dredge and removed was nearly constant regardless of nozzle size. The percentages of removal for the jet alone were also nearly constant. However, with the jet-dredge almost all of the fluidized material was removed while the jet alone only removed about one-quarter of the material.

(Text Continued on Page 24)

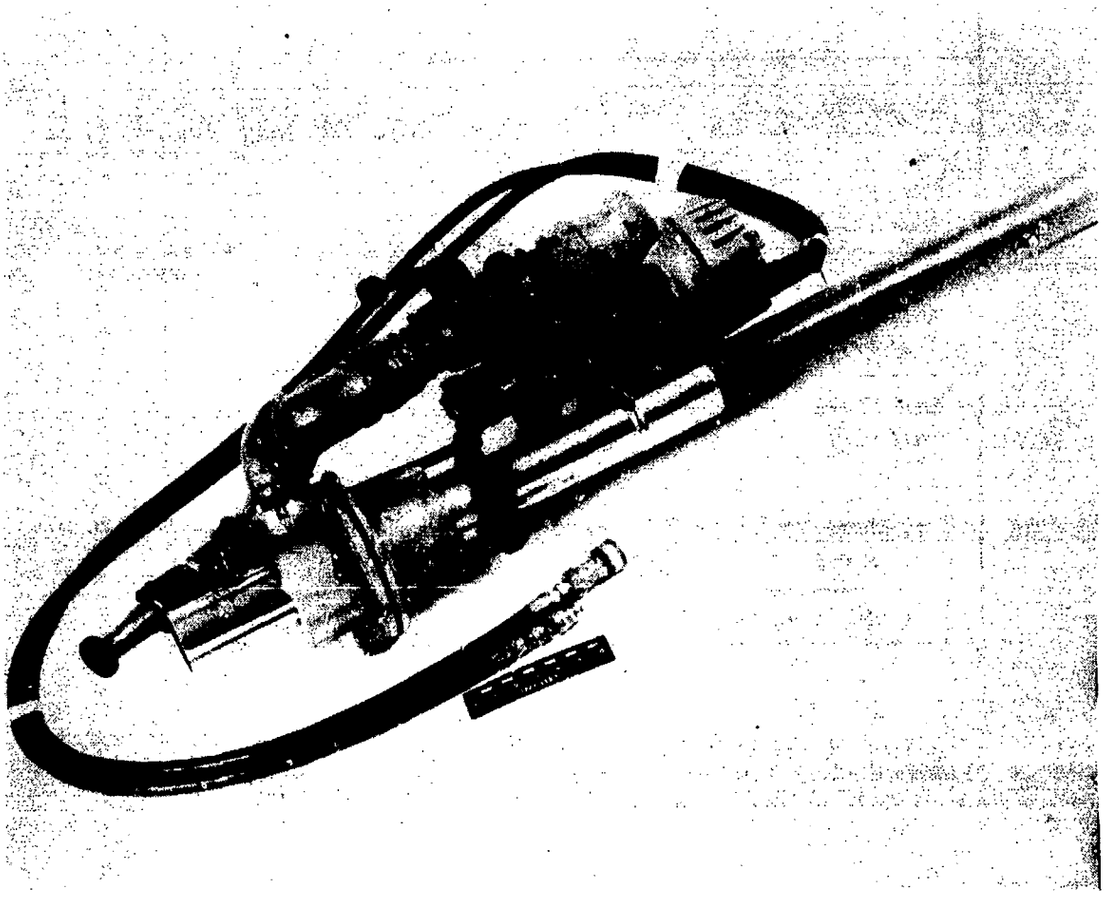

FIGURE 10. DREDGE SIDE OF JET-DREDGE TOOL

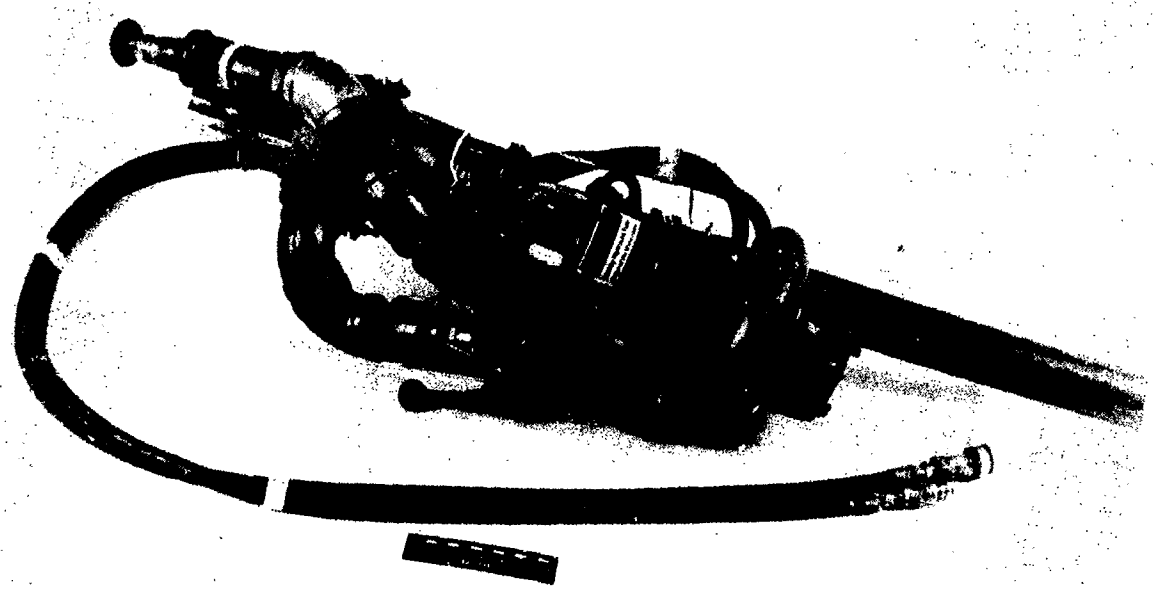

FIGURE 11. JET SIDE ET-DREDGE TOOL

TABLE 3

FLUIDIZATION/REMOVAL DATA

Nozzle Size (in.)	Jet: Volume Fluidized $(ft)^3$	Jet: Volume Fluidized (m^3)	Jet: Volume Removed (ft^3)	Jet: Volume Removed (m^3)	Jet: Excavation* Effectiveness (%)	Combined Jet-Dredge: Volume Fluidized (ft^3)	Combined Jet-Dredge: Volume Fluidized (m^3)	Combined Jet-Dredge: Volume Removed (ft^3)	Combined Jet-Dredge: Volume Removed (m^3)	Combined Jet-Dredge: Excavation Effectiveness (%)	Combined Jet-Dredge: Fluidization+ Effectiveness (%)
1 1/4	50	(1.4)	12.7	(0.36)	25	16	(0.45)	15.8	(0.45)	99	32
1	28	(0.8)	7.1	(0.2)	25	12	(0.34	11.6	(0.33)	97	43
3/8	15	(0.4)	3.9	(0.1)	26	9.4	(0.27)	9.0	(0.25)	96	63

Note: (1) Data taken off east pier at NCSC; sand was fine grained and included broken shells, small pebbles, etc.

(2) All tests were 1 minute duration.

* Volume removed as a percentage of volume fluidized.

\+ Volume fluidized by the jet-dredge as a percentage of the volume fluidized by the jet alone.

TABLE 4

CALCULATED AND MEASURED REACTION FORCES
FOR TAPERED NOZZLES

Nozzle (in.)	Hydraulic Fluid Flow Rate (gpm)	(lpm)	Water Flow Rate (ft^3/sec)	Reaction Force (Calculated) (lb)	(kg)	Reaction Force (Measured) (lb)	(kg)
1 1/4	10	(37.8)	0.49	56.2	(25.5)	57.1	(25.9)
	9		0.45	47.4		49.5	
	8		0.40	37.5		38.0	
	7		0.35	28.7		29.5	
	6		0.29	19.7		21.5	
	5	(18.9)	0.26	15.8	(7.2)	16.7	(7.6)
1 1/8	10	(37.8)	0.42	50.8	(23.0)		
	9		0.38	41.7			
	8		0.35	35.2			
	7		0.29	24.3		Not Measured	
	6		0.25	18.1			
	5	(18.9	0.21	12.7	(5.6)		
1	10	(37.8)	0.38	52.3	(23.4)	52.8	(23.9)
	9		0.32	37.1		38.2	
	8		0.28	28.4		29.1	
	7		0.25	27.6		28.2	
	6		0.21	15.9		16.5	
	5	(18.9)	0.17	10.5	(4.6)	11.0	(5)
3/4	10	(37.8)	0.22	31.1	(14.1)	24.9	(11.3)
	9		0.21	28.3		22.5	
	8		0.18	20.8		18.5	
	7		0.15	14.4		12.0	
	6		0.12	9.2	(4.2)	6.5	(2.9)
	5	(18.9)	-				
1/2	10	(37.8)	0.096	13.1	(5.9)		
	9		0.078	8.7			
	8		0.072	7.4		Nozzle	
	7		0.54	4.1		Lost During	
	6		0.45	2.9	(1.3)	Test	

In a soil removal operation the available energy must be proportioned between the jet and the dredge, consequently less material is fluidized. The net effect could be in either direction; in sandy soil; i.e.,; relatively heavy particles; there is a net increase in excavation rate, but in unconsolidated silt or clay the dredge's contribution may not be very pronounced.

In comparing the total fluidized volumes (fluidization efficiency) there is noted a systematic trend which may bear further investigation. No conclusions concerning this trend are drawn on the basis of the data in Table 3.

The jet-dredge combination shows many advantages over individual jet and dredge components:

1. Excavation rates were higher with the combination tool than with the jet alone. Although no quantitative data were taken using the dredge alone, experience has demonstrated that the dredge alone can easily become clogged if the diver gets its suction buried in sand. The combination tool does not have this problem because the jet is continually fluidizing the sediments in front of the dredge.

2. Visibility is greatly enhanced by adding the dredge to the jet. The dredge sucks up the cloud of silt raised by the jet thereby allowing the water to remain relatively clear. The dredge, used alone, presents no particular visibility problems.

3. Reaction forces are greatly reduced by combining the jet and the dredge. There is a residual moment due to the offset between the jet and dredge, but it is easily controlled by resting the tool on the sediment being excavated. Even this small imbalance could be eliminated by placing two jets symmetrically about the dredge suction.

DESIGN PROCEDURES

The tests seem to make it clear that much of the guesswork can be taken out of a jetting system design. However, to take advantage of the great advantages of the jet-dredge combination more design information on the dredge is required. Also, for systems which travel automatically across the seafloor, data are required to establish optimal speeds of travel. For diver operated systems it can be assumed that the diver will work slowly enough to jet the required depth before moving on.

A hypotehtical situation is described to illustrate the use of design procedures considered:

A heavy cable is to be buried to a depth of at least 38 inches (96.52 cm) in a sandy bottom having a shear strength of 0.2 psi (0.01 kg/m^2). It is assumed that the cable can be laid across the sand first, and buried later, and that, because of the instability of the soil, the diver will not push the jet into the soil, but rather will hold it at the surface. Finally, the cable is assumed to be heavy enough to sink through fluidized sand.

The first step is to determine what stagnation pressure is required at the bottom of the hole. While we found that the average stagnation pressure at the bottom of the hole was about three times the soil shear strength it would be wise to give the diver a little more pressure than required. For design purposes, let us choose five times the shear strength or 1.0 psi (0.07 kg/m^2).

The second step is to decide how to get this pressure. Since

$$P_s = \frac{P_o\ 47}{(\frac{x}{D} + 2.1)^2}$$

can be rearranged to give

$$P_s(x + 2.1D)2 = 47\ P_oD^2,$$

and since $x > 2.10$, the approximateion

$$P_s x^2 \approx 47\ P_oD^2$$

can be made. Substitution of numerical values then give

$$30.7\ \text{lbs} \approx P_oD^2 = \frac{P_s x^2}{47},$$

showing that an inverse relationship between the initial nozzle pressure and the nozzle area satisfies the constraint on stagnation pressure.

A further transformation is made possible by noting that flow rate and pressure are also related by the nozzle area. Each nozzle is characterized by a curve of the form

$$P_o = kQ^2$$

where k = constant characteristic to the nozzle's flow-pressure curve

which is more normally written

$$Q = C_Q A\sqrt{\frac{2\ P_o}{\rho}} = \frac{\pi D^2}{4}\ C_Q\sqrt{\frac{2\ P_o}{\rho}} \quad .$$

From this last equation

$$D^2 = \frac{4Q}{\pi C_Q\sqrt{\frac{\rho}{2P_o}}} \quad .$$

Now substitution into the equation

$$\frac{P_s x^2}{47} \approx P_o D^2$$

gives

$$\frac{P_s x^2}{47} \approx P_o\{\frac{4Q}{\pi C_Q\sqrt{\frac{\rho}{2P_o}}}\} \quad .$$

Rearrangement gives $P_o = \left(\frac{P_s x^2 \pi\ C_Q}{47\ (4\ Q)}\right)^2 \frac{2}{\rho}$, and substitution of the approximate values

$C_Q = 1.0$ Discharge Coefficient

$\rho = 2\ \frac{\text{lb-sec}^2}{\text{ft}^4}$

1 gallon = 231 in^3 (3785.4 cc)

yield a final numerical form which can be graphed:

$$P_o = \{8.1 \times 10^5/Q^2\}\ \{(\text{gpm})^2\ \text{psi}\} \quad .$$

From Figure 12, which shows this curve and several nozzle characteristic curves, it is obvious that several different nozzles are feasible.

In order to illustrate the futility of trying to minimize reaction forces on the diver without adversely affecting stagnation pressure at the bottom of the hole, the following controlling equation is presented

(Text Continued on Page 28)

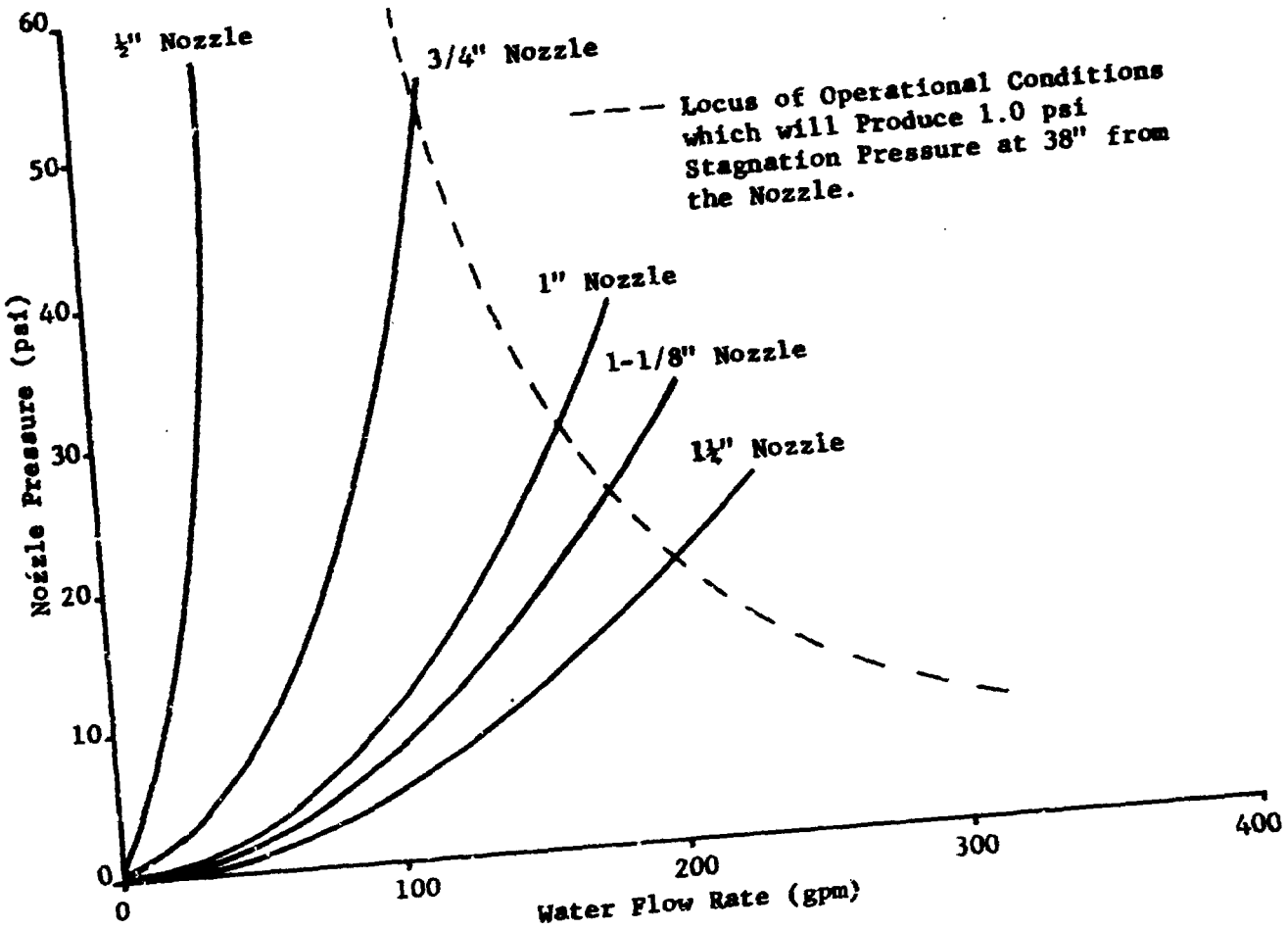

FIGURE 12. GRAPHIC SOLUTION FOR THE CABLE BURIAL PROBLEM

$$F = \frac{\rho Q^2}{A} = \frac{4\rho Q^2}{\pi D^2} .$$

Substitution of the equation

$$D^2 = \frac{4Q}{\pi C_Q \sqrt{\frac{\rho}{2P_o}}}$$

gives

$$F = \sqrt{2\rho}\ \ C_Q \sqrt{P_o}\ \ Q .$$

Solving for P_o gives

$$P_o = \frac{F^2}{2\rho C_Q^2 Q^2 \approx 910 \frac{F^2}{Q^2}} \quad \frac{psi(gpm)^2}{lb^2} .$$

Unfortunately, if F in this equation is fixed, the dependence of P_o on Q is precisely the same as it was for the equation which defines acceptable operating conditions:

$$P_o = \left\{ \left(\frac{P_s x^2 \pi C_Q}{4} \right)^2 (\tfrac{2}{\rho})/Q^2 \right\} .$$

In this example the association of 910 F^2 with 8.1×10^5 in the two equations for P_o leads inevitably to the conclusion that $F \approx 30$ lb (13.6 kg).

If this is unacceptable, perhaps a balanced nozzle should be considered. With such a configuration about twice the water flow rate is required to achieve the proper initial nozzle pressure; a larger power source may be required. Another alternative would be to weight the nozzle with about 30 lb of lead. This may be the least expensive solution.

Elimination of reaction forces in this type situation is not possible, however a solution which would yield a minimum horsepower available in the form

$$P_o = \frac{1714\ HP}{Q}$$

does not show the same functional form as

$$P_o = \{8.1 \times \frac{10^5}{Q^2}\} .$$

Minimizing horsepower, given by an equation of the form

$$HP = k_1 P_o Q$$

subject to the constraint that

$$P_o = \frac{k_2}{Q^2} ;$$

is the same as minimizing horsepower expressed in the form

$$HP = \frac{k_3}{Q} ;$$

there is no local extremum of horsepower. Therefore, to minimize horsepower within the constraint of hardware availability it is advantageous to use the nozzle that gives the highest flow rate. This is the largest nozzle whose characteristic curve intersects the locus of acceptable operating conditions within the capabilities of the pump.

The minimum horsepower solution is, however, of academic interest only because, for existing power supply and water pump hardware, the proper nozzle choice would be the one which gives the most margin against unanticipated patches of hard sediments. This amounts to choosing the nozzle which could, if used with the power source wide open, produce the greatest stagnation pressure at the desired burial depth. Recalling that

$$P_o = \left\{ \left(\frac{P_s x^2 \pi C_Q}{4} \right)^2 \frac{(\frac{2}{\rho})}{Q^2} \right\},$$

it is apparent that optimal jetting performance (in terms of fluidization) will be achieved when P_s is such that the curve described by the above equation is just tangent to the highest pump characteristic curve; the optimal nozzle is chosen on this basis. Figure 13 shows the 10 gpm (37.9 lpm) hydraulic fluid supply curve for the sump pump used during our experiments, several nozzle characteristic curves, and the operational curve ($P_o = k/Q^2$) which is just tangent to the pump curve. In this case, a nozzle size greater than 1 1/4 in. is indicated. If the 1 1/4 in. nozzle is the largest one available, then it should be chosen. Coincidently, in this example, the choice of the largest nozzle also minimizes horsepower.

The final design calculation to be covered is the relationship between nozzle size and the coefficient of the nozzles characteristic equation

$$Q = \frac{\pi D^2 C_Q}{4} \frac{2P_o}{\rho} .$$

(Text Continued on Page 31)

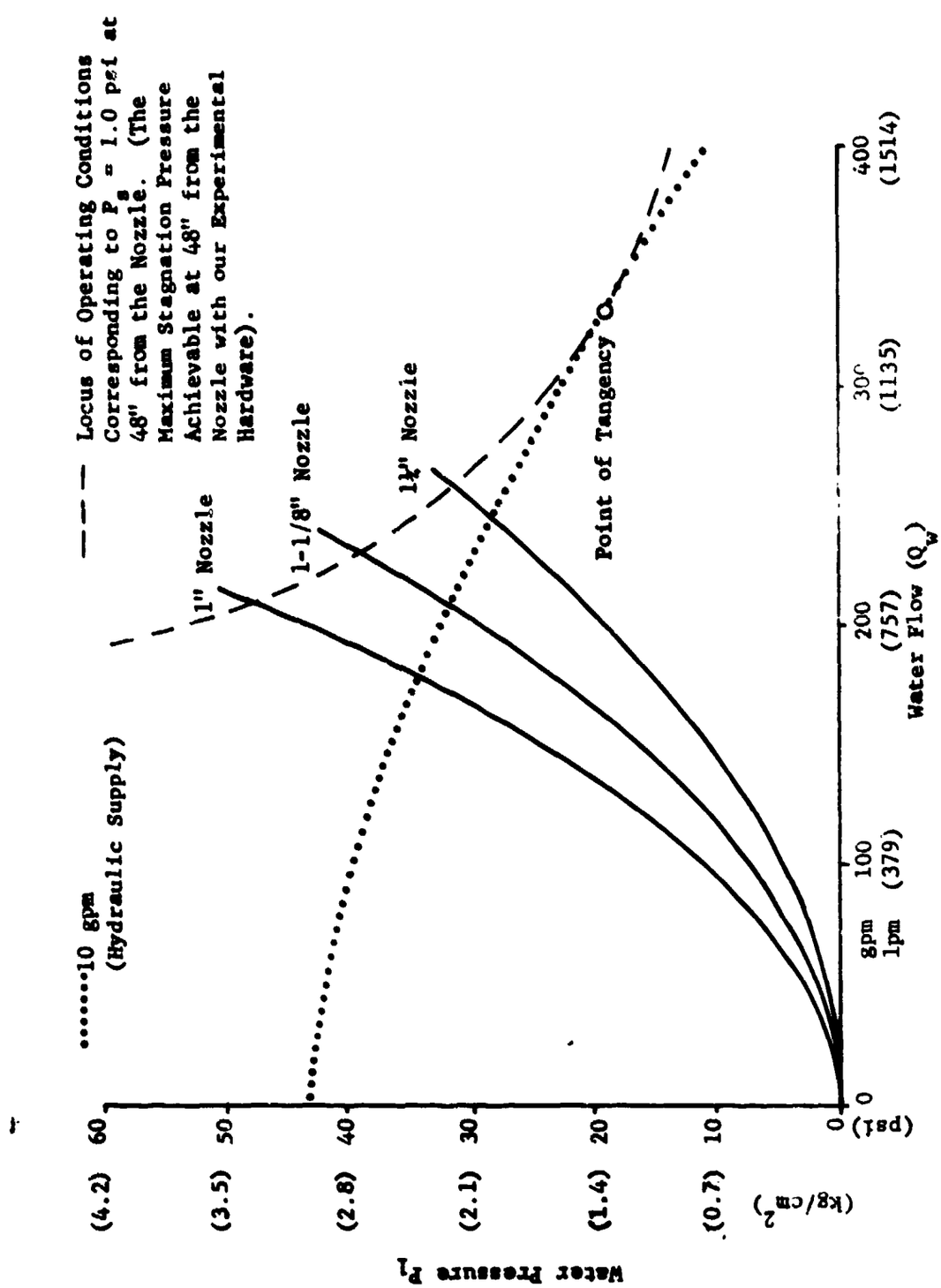

FIGURE 13. LOCUS OF MAXIMUM STAGNATION PRESSURES OBTAINABLE FROM EXPERIMENTAL HARDWARE

In the foregoing discussion, a value of 1.0 was used for C_Q; this discussion will rationalize the choice. If the equation is rearranged slightly it will read

$$P_o \left\{ \left(\frac{4}{\pi D^2 C_Q} \right)^2 \left(\frac{\rho}{2} \right) \right\} Q^2 .$$

Values of the coefficient,

$$\left(\frac{4}{\pi D^2 C_Q} \right)^2 \frac{\rho}{2} ,$$

have been calculated for each nozzle, on the basis of experimental data and are presented in Table 5. Since the constant (k) can be related to the nozzle diameter (D) through the equation

$$k = \frac{8\rho}{\pi^2 C_Q^2 D^4}$$

the value of C_Q can be found by fitting a straight line to data presented in the log-log form;

$$\ln k = \ln \left(\frac{8\rho}{\pi^2 C_Q^2} \right) - 4 \ln D .$$

Figure 14 shows these data graphically. From the least squares fit to the data, the intercept

$$\ln \left(\frac{8\rho}{(\pi^2 C_Q^2)} \right) ,$$

equals -6.76.

Taking the antilog

$$1.16 \times 10^{-3} = 8\rho/\pi^2 C_Q^2$$

from which

$$C_Q \quad 37.3 \left\{ \frac{\text{sec. gal}}{\text{ft}^2 \text{ in. min}} \right\} .$$

(Text Continued on Page 33)

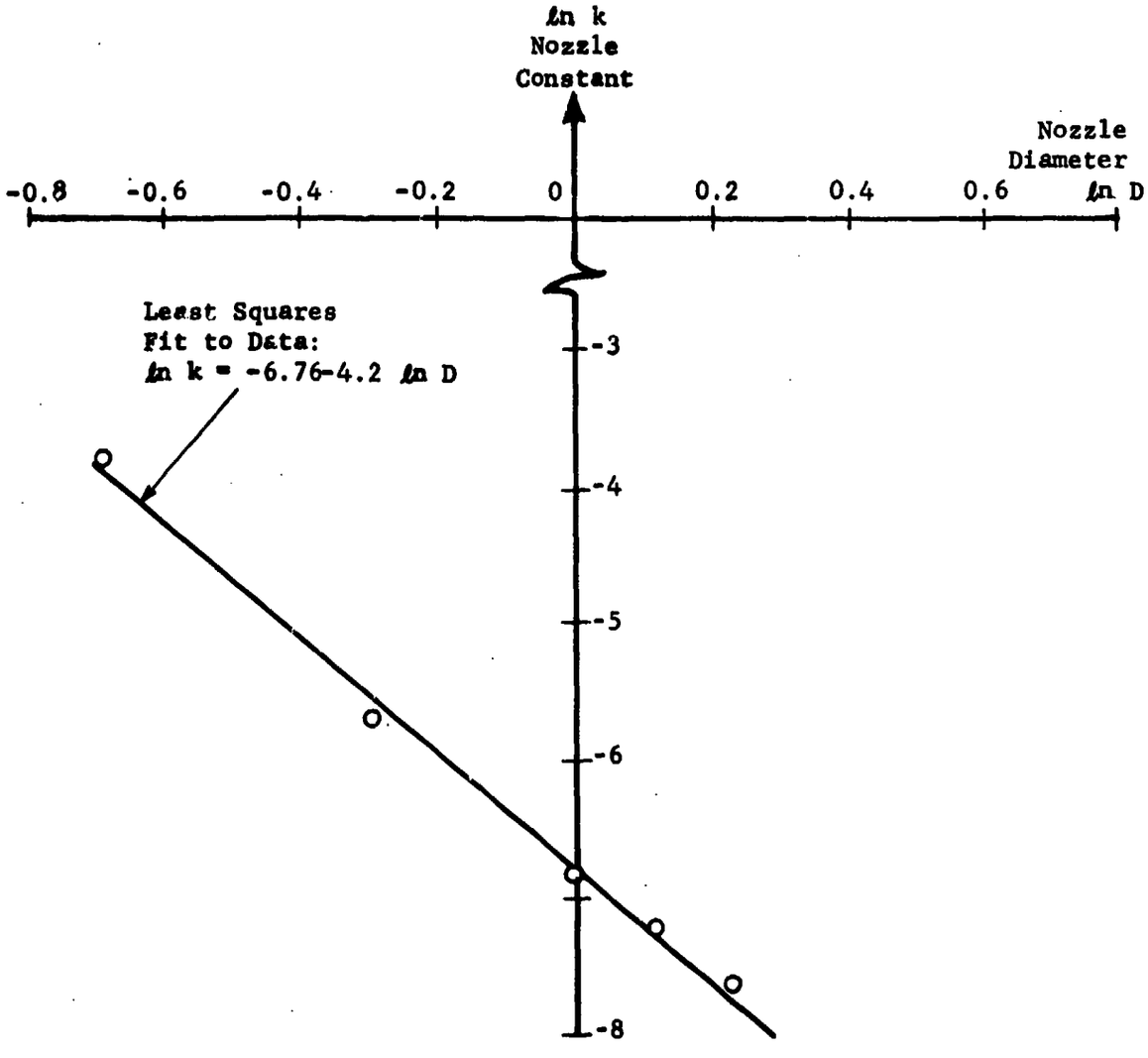

FIGURE 14. NOZZLE CONSTANT RELATED TO NOZZLE DIAMETER

TABLE 5

NOZZLE CONSTANTS

Nozzle Size (in.)	Constant (k) (psi/gpm^2)
1/2	2.38×10^{-2}
3/4	3.40×10^{-3}
1	1.11×10^{-3}
1 1/8	7.44×10^{-4}
1 1/4	4.77×10^{-4}

Applying the appropriate conversion factors to cancel the units of C_Q gives

$$C_Q \approx 1.0 .$$

The foregoing discussion covers the design of a single jet system intended for burial by fluidization. It applies virtually all of the quantitative results of this effort, but does not address the dredge at all. For applications requiring the actual removal of sediments, rather than just fluidized, the dredge is believed to be highly effective. However, not enough quantified information is presently available to present a systematic design procedure at this time.

CONCLUSIONS

Through the use of the jet/dredge, a diver was able to accomplish tasks involving trenching with greatly improved efficiency and ease. This device also allowed a diver to clearly monitor the progress of a task. Also, the diver, while performing his task, experienced minimal reaction forces from the device thus making it possible for a diver to continue working a particular task over an extended period of time without experiencing fatigue. This device is also compatible with the Model 2 power source.

After testing had been completed on the nozzles and pump, it was concluded that the optimum nozzle could be chosen which would produce the

maximum soil penetration, provided the soil shear strength was known. Also reaction forces could be calculated making it possible to predict forces which the user may experience.

RECOMMENDATIONS

Further studies in various types of soils should be carried out in order to relate nozzle size to soil characteristics. Also, the piping material should be constructed of lightweight aluminum pipe or tubing to decrease the weight of the device. Buoyancy should be attached directly to the device thus eliminating the tethered buoyancy package.

APPENDIX A

REACTION FORCE ANALYSIS

This appendix presents the mathematics which support the reaction force calculations in the body of the text. The important point is that only the change of momentum (not pressure) contributes to the reaction force. For example, consider a nozzle whose orifice is made smaller and smaller until finally it is closed. Then no matter how much pressure there is inside the nozzle, there will be no reaction force. Then a miniscule orifice certainly can't lead to large reaction forces, despite internal pressure; in fact, internal pressure has nothing to do with reaction forces, except by way of the nozzle's characteristic curve which relates flow rate to pressure drop.

Figure A1 shows a system for which reaction forces can easily be calculated on the basis of the very fundamental force balance

$$\vec{F} = m\vec{a} \ .$$

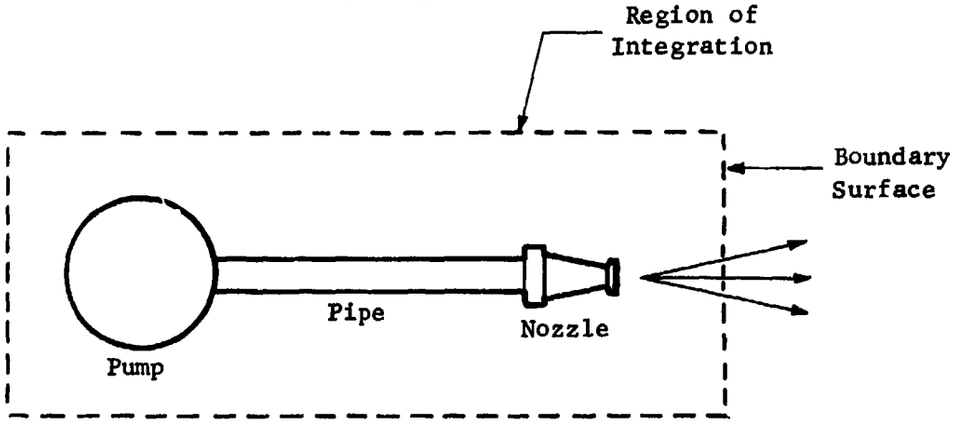

FIGURE A1. MATHEMATICAL MODEL OF TEST RIG

Applying this formula to small volume elements ($d\tau$) within the region indicated in Figure A1 gives Euler's equation

$$d\vec{F} = \rho \frac{D(\vec{V})}{Dt} d\tau$$

which is developed in all elementary fluid mechanics texts*. Integrating this force balance over the region of interest gives

$$\sum F_{\text{external}} = \int_R \rho \frac{D(\vec{V})}{Dt} d\tau \ .$$

The objective of further calculations is to reduce this very general formula to something that can be readily calculated. This will be accomplished by transforming the volume integral to a surface integral.

Recalling the equation of continuity

$$\frac{\partial \rho}{\partial t} + \text{div}(\rho \vec{V}) = 0$$

provides the key to this transformation. Multiplying the continuity equation by $\vec{V}$ gives

$$\vec{V} \frac{\partial \rho}{\partial t} + \vec{V} \ \text{div}(\rho \vec{V}) = 0 \ .$$

The projection of this equation on the *i*th axis gives

$$v_i \frac{\partial \rho}{\partial t} + v_i \ \text{div} \ \rho \vec{V} = 0 \ .$$

Now noting that

$$v_i \ \text{div} \ \rho \vec{V} = \text{div} \ v_i \ \rho \vec{V} - \rho \vec{V} \cdot \text{grad} \ v_i$$

allows this equation

$$v_i \frac{\partial \rho}{\partial t} + \vec{V} \cdot (v_i \ \rho \vec{V}) - \rho \vec{V} \cdot \vec{V} \ v_i = 0$$

to be combined with the *i*th component of the force balance,

---

*the notation $\frac{D\vec{V}}{Dt}$ is the particular derivative equal to

$$\frac{\partial \vec{V}}{\partial t} + (\vec{V} \cdot \vec{V}) \ \vec{V}$$

$$\rho \frac{\partial v_i}{\partial t} + \rho(\vec{v} \cdot \vec{\nabla})\, v_i = \frac{dF_i}{d\tau}$$

to give

$$(\rho \frac{\partial v_i}{\partial t} + v_i \frac{\partial \rho}{\partial t}) + \vec{\nabla} \cdot (v_i \rho \vec{v}) + (\rho(\vec{v} \cdot \vec{\nabla})\, v_i - \rho \vec{v} \cdot (\vec{\nabla} v_i)) = \frac{dF_i}{d\tau} \quad .$$

Finally, noting that

$$\rho(\vec{v} \cdot \vec{\nabla}) v_i = \rho \vec{v} \cdot (\vec{\nabla} v_i)$$

leads to the *ith* equation

$$\frac{\partial}{\partial} (\rho v_i) + \vec{\nabla} \cdot (v_i \rho\, \vec{v}) = \frac{dF_i}{d\tau} \quad .$$

Integrating this over the region shown in Figure A1 gives

$$\int_R \frac{\partial}{\partial t} (\rho v_i)\, d\tau + \int_R \vec{\nabla} \cdot (v_i \rho \vec{v})\, d\tau = (\Sigma F_{\text{external}})_i$$

and, applying the divergence formula

$$\int_R \vec{\nabla}\ \vec{B} d\tau = \int_S \vec{B} \cdot \eta d\sigma$$

gives the *ith* equation in a more useful form:

$$\int_R \frac{\partial}{\partial t} (\rho v_i)\, d\tau + \int_S v_i \rho \vec{v} \cdot \vec{\eta} d\tau = (\Sigma F_{\text{external}})_i \quad .$$

Recombination of the components gives the final equation

$$\int_R \frac{\partial}{\partial t} (\rho \vec{v}) d\tau + \int_S \rho \vec{v} (\vec{v} \cdot \vec{\eta})\, d\tau = \Sigma \vec{F}_{\text{external}}$$

which is the integral form of Euler's equation.

In the case of a submerged jet operating under steady condition the following assumption can be made:

$$\frac{\partial}{\partial t} \text{ is identically zero}$$

$\vec{v}$ is zero every where except across the jet's initial section, and here, it is equal to Q/A and is normal to the surface of integration.

The formula then reduces to

$$\rho V^2 A = ||\Sigma F_{external}||$$

in the direction of the jet velocity vector. Since this is the force required to keep the region stationary, the jet's reaction force is in the opposite direction and has the same magnitude, $\rho V^2 A$.

APPENDIX B

STAGNATION PRESSURE ANALYSIS

This appendix supports the equation

$$P_s = \frac{47\ P_o}{(x/D + 2.1)^2}$$

which describes the dependence of the jet's stagnation pressure on the distance (x) from the nozzle orifice. Figure B1 shows the nozzle and jet, and the coordinate system used for analysis. Early analyses of the spread of turbulence in submerged jets established, with ample support from experimental efforts, that velocity profiles in the main region of the jet are "self similar;" each profile is the same when plotted on coordinates of

$$\frac{u}{u_m} \text{ and } \frac{y}{x - sD}$$

where u_m is the velocity along the centerline, y is the distance from the centerline at which u is measured, and x-sD is the distance from the pole to the jet section at which u is measured. The constant -s is the pole position relative to the nozzle orifice.

Experimental evidence also shows that static pressure within the jet is virtually the same as the surrounding ambient pressure. For irrotational flow with invariant static pressure the integral form of the Navier Stokes equation (Bernouilli's equation) is used to show that the total momentum flux of the jet through any jet cross section is constant:

$$\int_0^r [2\pi y\, d\ u]\ u = \text{constant (independent of x)}$$

where r is the radius of the jet section in question.

Making use of the self similarity of jet profiles, the variable

$$\eta = y/x - sD$$

is introduced, along with the equation

$$\frac{u}{u_m} = f\ (y/x - sD)$$

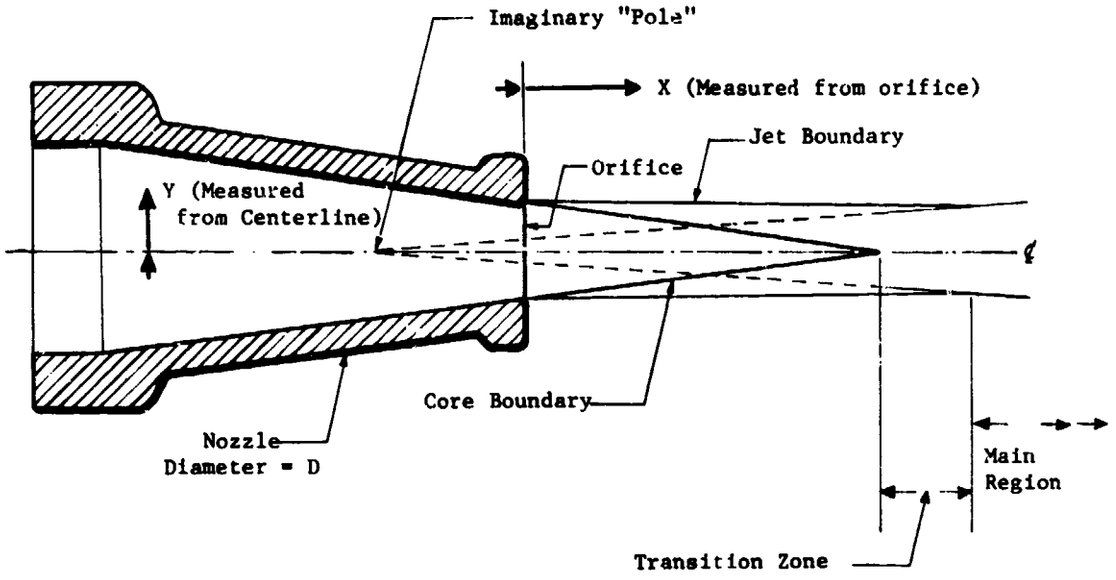

FIGURE B1. CROSS SECTION OF A SUBMERGED JET

to give

$$\int_0^{x/x-sD\,=\,\eta_{edge}} 2\pi(u_m f(\eta))^2\,(x - sD)^2\,\eta d\eta = \text{constant.}$$

Since x and u_m are explicitly independent of η, the equation can be rewritten as

$$u_m\,(x - sD)^2 \int_0^{\eta_{edge}} 2\pi f^2(\eta)\,\eta d\eta = \text{constant.}$$

Differentiation with respect to x gives

$$2(u_m\,(x - sD))\,\frac{d}{dx}\,(u_m(x - sD) \int_0^{\eta_{edge}} 2\pi f^2(\eta)\,\eta d\eta = 0$$

from which it is clear that

$$\frac{d}{dx}\,(u_m(x - sD)) = 0.$$

Hence,

$$u_m = \text{constant}/x - sD.$$

The last equation describes the decay of centerline velocity along the jet axis. Since static pressure is invariant, the stagnation pressure is directly proportional to u_m^2

$$P_s = \frac{\text{constant}}{(x - sD)^2} \quad .$$

Reference B1 continues to develop the momentum equation, and by evaluating terms at the nozzle orifice and at the start of the transition zone, arrives at values of the numerical constants which lead to the equation used in the body of this report

$$P_s = \frac{47.02\ P_o}{(x/D - 2.07)^2} \quad .$$

Experimental data from Reference B2 have been tested against these values by plotting

$$\sqrt{\frac{P_o}{P_s}} \text{ against } \frac{x}{D} \quad .$$

While the data tended to follow a straight line relationship, the numerical values extracted from linear regressions showed considerable spread around the predicted values in the equation.

$$\sqrt{\frac{P_o}{P_s}} = \frac{1}{\sqrt{47.02}}\left(\frac{x}{D} - 2.07\right) \quad .$$

Values corresponding to the figure, 47.02 typically came out between 42 and 68, while values corresponding to the figure -2.07 came out between -0.37 and +2.1. In applying the stagnation pressure equation in practice, the pole position is not very important since it is typically small by comparison to depths of fluidization.

(B1) Abramovich, G. N., *The Theory of Turbulent Jets*, M.I.T. Press, Cambridge, MA., 1963.

(B2) Cheung, J. B., et al, *Study on Water Jet Trenching, Flow Technology, Presentation #2*, Flow Research, Inc., Kent, Washington, 3 December 1976.

INITIAL DISTRIBUTION LIST

106	Commanding Officer, Harbor Clearance Unit ONE	(Copy 1)
	(Attn: OIC SDS-450)	(Copy 2)
	(ATTN: ENS G. T. Solether)	(Copy 3)
	(ATTN: BMCM R. Villasenor)	(Copy 4)
107	Commanding Officer, Harbor Clearance Unit TWO	(Copy 5)
	(ATTN: WO3 Leon Ryder)	(Copy 6)
---	Commanding Officer, Naval Construction Battalion Center, Davisville, RI 02854	
	(Code 10)	(Copy 7)
---	Commanding Officer, U. S. Naval Ship Repair Facility, Subic Bay, FPO San Francisco 96651	
	(ATTN: Diving Officer)	(Copy 8)
---	Commanding Officer, U. S. Naval Ship Repair Facility, FPO Seattle 98762	
	(ATTN: Diving Officer)	(Copy 9)
236	Commanding Officer, David Taylor Naval Ship R&D Center	
	(Code 1933, Mr. Jim Lee)	(Copy 10)
102	Commanding Officer, Naval Submarine Training Center, Pacific	
	(Code 60, Dir. of Diving and Escape)	(Copy 11)
580	Commander, Naval Construction Battalions, Atlantic	(Copy 12)
---	Commander, Cruiser Destroyer Force, Seventh Fleet, FPO San Francisco 96601	
	(ATTN: Diving Officer)	(Copy 13)
---	Commander, Naval Construction Battalions, Pacific Fleet, FPO San Francisco 96610	(Copy 14)
427	Commander, Naval Sea Systems Command	
	(ATTN: SEA 00C)	(Copies 15-20)
---	Commander, Service Force, U. S. Atlantic Fleet, Norfolk VA 23511	
	(ATTN: LCDR K. A. Gustafson)	(Copy 21)
383	Commander, Service Squadron 8, Norfolk	(Copy 22)
---	Commander, Submarine Squadron FOUR, FPO New York 09501	
	(ATTN: Material Officer)	(Copy 23)
---	Commander, Underwater Construction Team ONE, U. S. Naval Amphibious Base, Little Creek, Norfolk, VA 23512	(Copy 24)
---	Commander, Underwater Construction Team TWO, U. S. Naval Construction Battalion Center, Port Hueneme, CA 93043	(Copy 25)
---	USS PIGEON (ASR-21), FPO San Francisco 96601	(Copy 26)
---	T. L. Apjohn II, Commanding Officer, HCU-1001, Portsmouth, NH	(Copy 27)
197	Naval Explosive Ordnance Disposal Facility, Indian Head	
	(ATTN: E. Faccini, Code 5044)	(Copy 28)
---	USS COUCAL (ASR-8), FPO San Francisco 96601	(Copy 29)
---	National Oceanic and Atmospheric Administration, Rockville, MD 20852	
	(ATTN: Office of Coastal Environment, Code MR-6)	(Copy 30)
204	Naval Medical Research Institute, Natl. Naval Medical Center	(Copy 31)
186	Civil Engineering Laboratory, Naval Construction Battalion Center	(Copies 32-43)

---	National Marine Research Center, Box 1600, Galveston, TX 77550	(Copy 44)
124	Long Beach Naval Shipyard, Long Beach, CA (ATTN: Code 400, Public Works Dept., Diving Supervisor)	(Copy 45)
---	Naval Facilities Engineering Command, 200 Stovall St., Alexandria, VA 22332 (ATTN: Code PC-2, Ocean Facilities Program, CDR K. K. Donovan, CEC, Director)	(Copy 46)
288	Operational Test and Evaluation Force, Pacific	(Copy 47)
478	Commander, Naval Surface Force, Pacific	(Copy 48)
---	CAPT E. B. Mitchell, USN(Ret), 5403 Albemarle, Westmoreland Hills, MD	(Copy 49)
---	Naval Undersea Center, P. O. Box 997, Kailua, Hawaii 96734	(Copy 50)
---	Bill Nix, P. O. Box 4117, Pasadena, TX 77502	(Copy 51)
---	Ramsey Parks, Santa Barbara City College, 312 Nopal St., Santa Barbara, CA 93103	(Copy 52)
---	LCDR Lloyd L. Reynolds, USNR(R), 926 Springmill Rd., Villanova, PA 19085	(Copy 53)
---	George Sampson, DIVEX, 2245 Breaux Ave., P. O. Box 504, Harvey, LA 70058	(Copy 54)
---	George Scholley, Alcoa Marine Corporation, 1200 Ring Bldg., Washington, DC 20036	(Copy 55)
---	Vernon E. Shelton, Deep Ocean Work Systems, 645 E. 219th St., Unit 647, Carson, CA 90745	(Copy 56)
---	Robert J. Shourot, President, Undersea Systems, Inc., 112 W. Main St., Bay Shore, NY 11796	(Copy 57)
309	Submarine Development Group One	(Copy 58)
265	Commander, Naval Oceans Systems Center, San Diego (ATTN: Code 63, H. R. Talkington)	(Copy 59)
528	Mr. J. F. Freund, Naval Sea Systems Command (Code C353)	(Copy 60)
298	Portsmouth Naval Shipyard, Portsmouth, NH (ATTN: LCDR L. C. Gies)	(Copy 61)
---	D. Michael Hughes, Oceaneering International, Inc. 9219 Katy Freeway, Houston, TX 77024	(Copy 62)
---	Jim Joiner, Director, Commercial Diving Center, 272 S. Fries Ave., Wilmington, CA 90744	(Copy 63)
226	Naval School, Explosive Ordnance Disposal, Naval Ordnance Station, Indian Head	(Copy 64)
---	LCDR J. V. Khellman, USNR(R), Rt. #1, Henniker, NH 03242	(Copy 65)
---	Bob Kutzleb, Seaward, Inc., 6269 Leesburg Pike, Falls Church, VA 22044	(Copy 66)
---	Dick Long, Diving Unlimited, 1148 Delevan Drive, San Diego, CA 92102	(Copy 67)
299	Puget Sound Naval Shipyard, Bremerton (ATTN: Code 2125, Engineering Library)	(Copy 68)
---	CAPT Joseph Madeo, Murphy Pacific Salvage Corp., Maritt Division, 1 World Trade Center, Fleet 8833, New York 10048	(Copy 69)
---	Raymond F. McAllister, Prof. of Ocean Engineering, Florida Atlantic University, Boca Raton, FL 33432	(Copy 70)
229	Fleet & Mine Warfare Training Center, Charleston (ATTN: LCDR McConnochie)	(Copy 71)
---	Jim McDole, Taylor Diving & Salvage Co., 795 Engineering Rd., Belle Chasse, LA 70037	(Copy 72)

---	W. Tessin, Chairman, Florida Atlantic University, Dept. of Ocean Engineering, Boca Raton, FL 33432	(Copy 73)
---	E. A. Wardwell, Seaward. Inc., 6269 Leesburg Pike, Falls Church, VA 22044	(Copy 74)
289	Commander, Operational Test & Evaluation Force, Atlantic	(Copy 75)
---	Joanne Hills, Managing Editor FACEPLATE, Potomac Research Institute, 7655 Old Springhouse Rd., Westgate Research Park, McLean, VA 22104	(Copy 76)
35	Battelle Memorial Institute, Columbus Laboratories (ATTN: Don Hackman)	(Copy 77)
555	Naval Facilities Engineering Command, Chesapeake Div.	(Copy 78)
479	Norfolk Naval Shipyard, Portsmouth	(Copy 79)
340	Woods Hold Oceanographic Institution (ATTN: LO-206, Document Library)	(Copy 80)
23	Army Engineers Waterways Experiment Station, Vicksburg (ATTN: Library)	(Copy 81)
457	Oceanographer of the Navy (ATTN: Management Information Division)	(Copy 82)
257	Naval Submarine Base, New London (ATTN: Diving Supervisor)	(Copy 83)
45	Charleston Naval Shipyard (ATTN: Diving Supervisor)	(Copy 84)
125	Mare Island Naval Shipyard, Vallejo, CA (ATTN: Diving Supervisor)	(Copy 85)
216	Naval Ordnance Station, Indian Head (ATTN: Diving Supervisor)	(Copy 86)
297	Philadelphia Naval Shipyard, Philadelphia (ATTN: Diving Supervisor)	(Copy 87)
298	Portsmouth Naval Shipyard (ATTN: Diving Supervisor)	(Copy 88)
222	Naval Postgraduate School, Monterey (ATTN: Code 2124, Library)	(Copy 89)
---	Supervisor of Salvage, West Coast Representative, Bldg 7, Rm 82, Naval Station, Treasure Island, San Francisco 94130	(Copy 90)
485	Naval Ship Engineering Center, Hyattsville (ATTN: Technical Library)	(Copy 91)
491	Commander, Naval Oceans Systems Center (ATTN: Library)	(Copy 92)
---	Technical Processes Branch, D-823, NOAA Libraries Division, Rm 806, Silver Spring, MD 20910	(Copy 93)
208	Naval Oceanographic Office (ATTN: Code 600, Library)	(Copy 94)
---	Commanding Officer, USS AJAX (AR-6), Sasebo, FPO SF 96601 (ATTN: Diving Officer)	(Copy 95)
---	Commanding Officer, USS BRYCE CANYON (AD-36), Pearle, FPO SF 96601 (ATTN: Divi ~ Officer)	(Copy 96)
---	Commanding Officer, USS CAMOPUS (AS-34), Holy Loch, FPO NY 09501 (ATTN: Diving Officer)	(Copy 97)
---	Commanding Officer, USS DIXIE (AD-14), San Diego, FPO SF 96601 (ATTN: Diving Officer)	(Copy 98)

---	Commanding Officer, USS HECTOR (AR-7), San Francisco FPO SF 96601 (ATTN: Diving Officer)	(Copy 99)
---	Commanding Officer, USS HOLLAND (AS-32), Charleston FPO NY 09501 (ATTN: Diving Officer)	(Copy 100)
---	Commanding Officer, USS HUNLEY (AS-31), Charleston FPO NY 09501 (ATTN: Diving Officer)	(Copy 101)
---	Commanding Officer, USS ORIOR (AS-18), Charleston FPO NY 09501 (ATTN: Diving Officer)	(Copy 102)
---	Commanding Officer, USS PIEDMONT (AD-17), Naples FPO NY 09501 (ATTN: Diving Officer)	(Copy 103)
---	Commanding Officer, USS PRAIRIE (AD-15), San Diego FPO SF 96601 (ATTN: Diving Officer)	(Copy 104)
---	Commanding Officer, USS SAMUEL GOMPERS (AD-37), San Diego FPO SF 96601 (ATTN: Diving Officer)	(Copy 105)
---	Commanding Officer, USS SIERRA (AD-18), Charleston FPO NY 09501 (ATTN: Diving Officer)	(Copy 106)
---	Commanding Officer, USS SPERRY (AS-12), San Diego FSPO San Diego 92132 (ATTN: Diving Officer)	(Copy 107)
---	Commanding Officer, USS VULCAN (AR-5), NORVA, FPO NY 09501 (ATTN: Diving Officer)	(Copy 108)
---	Naval Ocean Systems Center, Diving Division, Long Beach, CA 90822 (ATTN: LT. O. Dunn)	(Copy 109)
75	Director, Defense Documentation Center	(Copies 110-121)